Smart Materials and Structures

PURPOSE-LED PUBLISHING™

TOPICAL REVIEW

Metamaterial-enabled guided wave manipulation: a novel paradigm for structural health monitoring

To cite this article: Shengbo Shan *et al* 2026 *Smart Mater. Struct.* **35** 063003

View the article online for updates and enhancements.

You may also like

- Collision enhanced hyper-damping in nonlinear elastic metamaterial
Miao Yu, , Xin Fang et al.

- Spider web-structured labyrinthine acoustic metamaterials for low-frequency sound control
A O Krushynska, F Bosia, M Miniaci et al.

- Elastic metamaterials for guided waves: from fundamentals to applications
Jeseung Lee and Yoon Young Kim

This content was downloaded from IP address 158.132.13.200 on 29/06/2026 at 06:40

Smart Materials and Structures

Check for updates

RECEIVED
14 February 2026

REVISED
23 May 2026

ACCEPTED FOR PUBLICATION
15 June 2026

PUBLISHED
29 June 2026

TOPICAL REVIEW

Metamaterial-enabled guided wave manipulation: a novel paradigm for structural health monitoring

Shengbo Shan[1,2,6,*], **Ze Liu**[3,6], **Yue-Sheng Wang**[4] **and Li Cheng**[3,5,*]

[1] College of Intelligence Science and Technology, National University of Defense Technology, Changsha 410073, People's Republic of China
[2] National Key Laboratory of Equipment State Sensing and Smart Support, National University of Defense Technology, Changsha 410073, People's Republic of China
[3] Department of Mechanical Engineering, The Hong Kong Polytechnic University, Kowloon, Hong Kong Special Administrative Region of China, People's Republic of China
[4] Department of Mechanics, School of Mechanical Engineering, Tianjin University, Tianjin 300350, People's Republic of China
[5] Hong Kong Branch of National Rail Transit Electrification and Automation Engineering Technology Research Center, The Hong Kong Polytechnic University, Kowloon, Hong Kong Special Administrative Region of China, People's Republic of China
[6] The authors have contributed equally and are designated as first authors.
[*] Authors to whom any correspondence should be addressed.

E-mail: shanshengbo25@nudt.edu.cn and li.cheng@polyu.edu.hk

Keywords: structural health monitoring, guided waves, elastic metamaterial, nonlinearity, wave manipulation

Abstract

Engineering structures are susceptible to damage throughout their service life, posing serious risks to structural integrity without timely awareness and action. To tackle the problem, guided wave-based structural health monitoring (GW-SHM) has emerged as a prominent technique for real-time condition assessment, owing to its sensitivity to damage and the ability for large-area inspection. GW-SHM methodologies can be categorized into linear and nonlinear approaches exhibiting various degrees of sensitivity to damage. Nevertheless, practical deployment of these techniques, especially the nonlinear ones which are known to be conducive to incipient damage detection, is hampered by considerable challenges in the generation, propagation, and reception of ultrasonic GWs, which stem from complex wave dynamics like wave dispersion, attenuation, and mode conversion. Elastic metamaterials (EMs), characterized by engineered sub-wavelength microstructures and tailored spatial distributions, offer a transformative strategy for wavefield manipulation, exemplified by bandgaps, beam steering, and mode conversion. This exceptional wave-manipulation capability positions EMs as a powerful tool to empower GW-SHM systems with unprecedented capability. This paper provides a systematic review and analysis of the recent advancements in the integration of metamaterial design and GW-SHM technology. After a concise discussion of the theoretical framework on linear and nonlinear GW propagation, we elucidate the fundamental mechanisms through which EMs exert control over GWs. We then critically address the specific requirements for wave manipulation across the complete GW-SHM chain, from actuation and propagation to sensing, for both linear and nonlinear techniques. A detailed discussion of bespoke EM designs, engineered to meet these distinct requirements, is presented, highlighting their demonstrated performance and potential impact on improving monitoring robustness and damage detection sensitivity. The integration of EMs into GW-SHM not only offers a new paradigm for achieving next-generation GW-SHM systems but also reciprocally inspires innovative pathways in the design and application of functional metamaterials.

1. Introduction

Engineering structures like aircraft panels, wind turbine blades, and petroleum pipelines are susceptible to a wide range of structural and material damages. These damages do not occur abruptly but evolve progressively, exhibiting diverse manifestations at different stages. In the early-stage initiation phase,

© 2026 IOP Publishing Ltd. All rights, including for text and data mining, AI training, and similar technologies, are reserved.

subtle yet critical changes take place. For example, high-cycle fatigue [1–3], induced by repeated loading, gradually undermines the material at the microscopic level. Local plastic zones [4–6] then form as the material undergoes permanent deformation under stress, deteriorating its mechanical properties. Concurrently, microstructural changes, such as atomic dislocation and void formation [7, 8], compromise the material properties for which they are designed. These incipient signs are often imperceptible to naked eyes, concealed within material's intricate microstructures. As damaging factors persist, the damage evolves to a more visible stage in which physical defects emerge, including cracks that traverse the material, fissures that resemble open wounds, and delamination where structural layers separate [9, 10]. These defects not only degrade the appearance of structures but also significantly reduce their load-bearing capacity and safety. If left undetected and unaddressed in a timely manner, such degradation can be detrimental and ultimately lead to catastrophic structural failure, resulting in critical economic losses, service disruptions, and even loss of lives, especially for large-scale structures.

To mitigate these risks and ensure the long-term safety and reliability of engineering structures, structural health monitoring (SHM) [11–15] has become an indispensable tool to develop. Unlike traditional inspection methods that are often time-consuming, labor-intensive, and may require shutdown of entire systems, SHM allows for online and real-time inspection, thereby continuously monitoring structural conditions and providing instant feedback on any changes or abnormalities. Based on diverse physical mechanisms, various SHM approaches have been developed, including static strain/deformation analysis [16], vibration frequency & mode assessment [17], acoustic emission detection [18, 19], eddy current inspection [20], electromechanical impedance measurement [21], and ultrasonic elastic wave probing [11, 22, 23] etc. Among these approaches, the guided wave (GW)-based method has attracted extensive research attention owing to its remarkable advantages over conventional techniques [24–29]. GWs refer to elastic waves that propagate within bounded waveguides such as plates, pipes, and rods which are widely used in engineering structures. Ultrasonic GWs can propagate over long distances within a structure, offering a broad detection range and reducing the number of sensors required. Moreover, GW-SHM methods consume relatively low energy during inspection, making them an energy-efficient solution. Most importantly, GWs are sensitive to damage, enabling the early detection of even small defects like micro-cracks or incipient microstructural changes [30–33].

GW-SHM techniques can categorically be classified into linear and nonlinear methods, contingent upon the use of GW components and the exploitation of their interaction with structural damages. Linear methods primarily rely on damage-induced phenomena that manifest as distinct alterations in wave propagation behavior, including wave reflection, scattering, variations in propagation velocity and wavenumber, and mode conversion [24–26, 34, 35]. These characteristic signatures are captured by sensors which are strategically integrated within the structure. Subsequently, the acquired data undergoes post-processing and diagnostic analysis to identify and locate damage. Notably, the manifestation of these phenomena is intrinsically linked to the wavelength of GWs, which should be smaller or on the same scale as the defects. In practical engineering applications, the wavelength of GWs in use typically falls within the millimeter range, thereby confining linear methods' efficacy to the detection of macroscale defects, such as visible cracks or significant material loss [36–42].

In stark contrast, nonlinear GW-SHM methods [7, 43–48] exploit the interaction between probing waves and damage through the inherent nonlinearities associated with microstructural imperfections within the material like lattice anomalies, dislocations, and microcracks which introduce nonlinear stress–strain relationships. This interaction leads to an energy transfer from the fundamental frequency of the probing waves to other frequencies, exemplified by the generation of higher harmonics (integer multiples of the fundamental frequency) [49, 50], subharmonics (fractional multiples of the fundamental frequency) [51, 52], quasi-static components (low-frequency components close to zero frequency) [53, 54], and combinational harmonics (sum and difference of the fundamental frequencies) [55–57]. The presence of these nonlinear features serves as a sensitive indicator of material microstructural degradations and micro-scale damage, which may not be detectable by linear methods. Consequently, nonlinear GW-SHM methodologies offer significantly enhanced sensitivity to early-stage damage and subtle changes in material properties, enabling the detection of incipient defects before they evolve into macroscale or visible damages.

In practical applications, several critical issues associated with GW generation, propagation, and reception significantly impede the practical implementation of both linear and nonlinear GW-SHM techniques. In linear GW-SHM, GWs inherently exhibit multi-modal and dispersive characteristics [11]. At a specific excitation frequency, multiple GW modes can be generated, each propagating at different velocities. Concurrently, the propagation velocities of wave modes are frequency-dependent, further complicating their exploitation for SHM applications. These inherent characteristics markedly elevate the complexity of the response signals, thereby posing substantial challenges for the accurate extraction of damage features [58, 59]. Moreover, certain types of GW modes possess unique attributes that are particularly advantageous for SHM applications, yet they are difficult to generate. For instance, shear horizontal (SH) waves in plate-like structures are shown to be immune to energy leakage into surrounding fluids, making them highly desirable for certain monitoring scenarios [60–62]. However, the excitation of SH waves in plates proves to be much more difficult compared to Lamb waves [62]. In the realm of nonlinear GW-SHM, the damage-related nonlinear wave components are typically weak due to the incipient nature of damage [46]. Consequently, the measurement of nonlinear GWs is highly susceptible to interference from various extraneous non-damage-related factors. For example, nonlinear sources from instruments, transducers, and their corresponding installations inevitably exist within any real-life SHM system, potentially overshadowing the actual damage-related information and leading to erroneous interpretations [44, 63]. Furthermore, other unavoidable factors inherent in practical applications exacerbate the signal complexity. Examples include the coexistence of multiple wave modes [64], energy weakening induced by wave divergence [65], and boundary reflections [66, 67], etc. Collectively, these factors render the extraction of damage features from nonlinear GW signals highly challenging, thereby limiting the overall reliability and efficacy of the nonlinear GW-SHM techniques.

The aforementioned challenges underscore a pressing need for the formulation of a comprehensive wave manipulation strategy, encompassing all critical stages in an SHM cycle, ranging from wave generation, propagation, to reception, with the ultimate goal of enhancing the performance of GW-SHM methods and increasing their applicability. The underlying rationale consists of leveraging the concept of metamaterials to achieve strategic and precise wave manipulation. Metamaterials [68], as artificial functional media meticulously structured at the subwavelength scale, have demonstrated immense potential in manipulating electromagnetic [69–71], acoustic [72–74], and elastic waves [75–80] with unprecedented design space and precision. Specifically, through the strategic control of vector waves, elastic metamaterials (EMs), characterized by their precisely tailored microstructures and distribution patterns, allow for the creation of a diverse array of effective material parameter combinations [81, 82]. This, in turn, gives rise to a variety of unconventional wave phenomena, including but not limited to bandgaps [83, 84], negative/zero refraction [77, 85], non-reciprocity [86, 87], self-collimation [88], and wavefront steering [89–91]. Owing to their exceptional capability for wave manipulation, EMs are poised to significantly enhance existing GW-SHM methodologies. Through engineering GW generation, propagation, and reception, EMs would allow for enhancing wave-damage interactions and facilitating the extraction of subtle damage-induced features. Consequently, the integration of EMs into GW-SHM frameworks represents a promising technological breakthrough in advancing the field of SHM.

To reflect the state-of-the-art in this field, this review meticulously examines the most recent advancements in metamaterial-enabled GW-SHM techniques, encompassing both linear and nonlinear methodologies. The overall framework is illustrated in figure 1. First, the theory of linear and nonlinear GWs is briefly reviewed to establish the foundation for subsequent discussions. Then, we provide a brief overview of typical wave manipulation phenomena and underlying mechanisms exhibited by EMs. This includes an in-depth analysis of how EMs, through their precisely engineered microstructures and distribution patterns, can give birth to a wide range of unconventional wave behaviors, which are pivotal for their further SHM applications. Subsequently, the review delves into the specific requirements for wave manipulation in the context of both linear and nonlinear GW-SHM approaches. We elucidate how these requirements dictate the design principles of EMs, highlighting the necessity for tailored microstructural configurations to achieve the desired performance. Detailed designs of EMs, tailored to meet the specific demands of linear and nonlinear GW-SHM, are presented and discussed in detail, underscoring their potential to significantly improve damage detection sensitivity and accuracy. Finally, conclusions are drawn based on the presented findings, alongside discussions on future research directions to highlight the transformative potential of EMs in advancing GW-SHM technologies and possible avenues for further exploration.

2. Theoretical basis of linear and nonlinear GWs

When elastic waves propagate in isotropic solid waveguides, like thin-walled plates or pipes, GWs are generated due to the coupling of forward and reflected waves [11]. Taking a plate structure as a representative case, GWs are primarily categorized into Lamb waves and SH waves based on the polarization direction of particle motion, as shown in figure 2(a), respectively. Also, symmetric (S) and antisymmetric (A) modes are generated due to the displacement distribution across the plate thickness, as shown in figure 2(b). When the medium contains material nonlinearity (e.g. plasticity [4, 5]) or contact acoustic

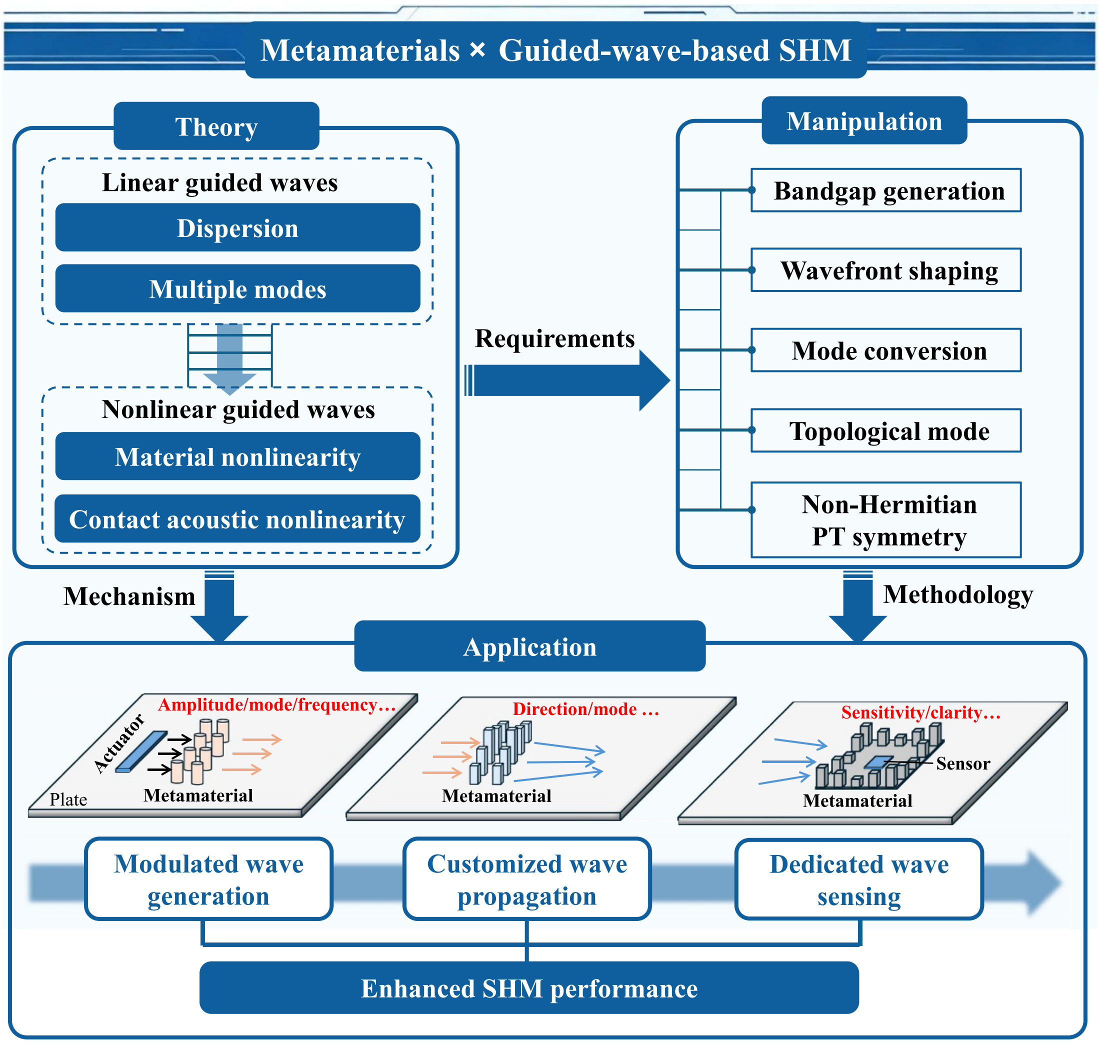

Figure 1. Framework of the review.

nonlinearity (e.g. crack [92, 93]), nonlinear GWs, such as higher harmonics and sub-harmonics, are generated.

This section aims to establish the theoretical foundation for GW-SHM. It begins with the fundamentals of linear GWs in thin-walled, isotropic plates, encompassing their governing equations, dispersion relations, and mode shapes. Building upon this, the discussion proceeds to the physical mechanisms governing nonlinear GW generation, primarily higher-order harmonics and wave mixing.

2.1. Linear GWs

GWs in isotropic plates are first discussed. Owing to their intrinsic decoupling, Lamb waves and SH waves are addressed in separate derivations.

Lamb wave problems (in x–z plane) can be treated as the coupling of both pressure waves and shear vertical waves. A general governing equation, derived from the combination of equilibrium equation, constitutive (stress–strain) equation, and geometry (strain-displacement) relation, can be expressed with two potential functions, ϕ and ψ, as [94–96]

$$\begin{cases} \frac{\partial^2\phi}{\partial x^2}+\frac{\partial^2\phi}{\partial z^2}=-\frac{\omega^2}{c_{\mathrm{P}}^2}\phi \\ \frac{\partial^2\psi}{\partial x^2}+\frac{\partial^2\psi}{\partial z^2}=-\frac{\omega^2}{c_{\mathrm{S}}^2}\psi \end{cases}, \tag{1}$$

where $c_{\mathrm{P}}^2=(\lambda+2\mu)/\rho$ and $c_{\mathrm{S}}^2=\mu/\rho$ represent the velocities of pressure and shear waves, respectively. λ and μ are Lamé constants. ρ denotes mass density. ω is angular frequency. Specifically, for Lamb waves propagating in the x direction, ϕ and ψ have the following forms, respectively,

$$\phi=f(z)\,\mathrm{e}^{i(kx-\omega t)},\psi=\mathrm{i}h(z)\,\mathrm{e}^{\mathrm{i}(kx-\omega t)}, \tag{2}$$

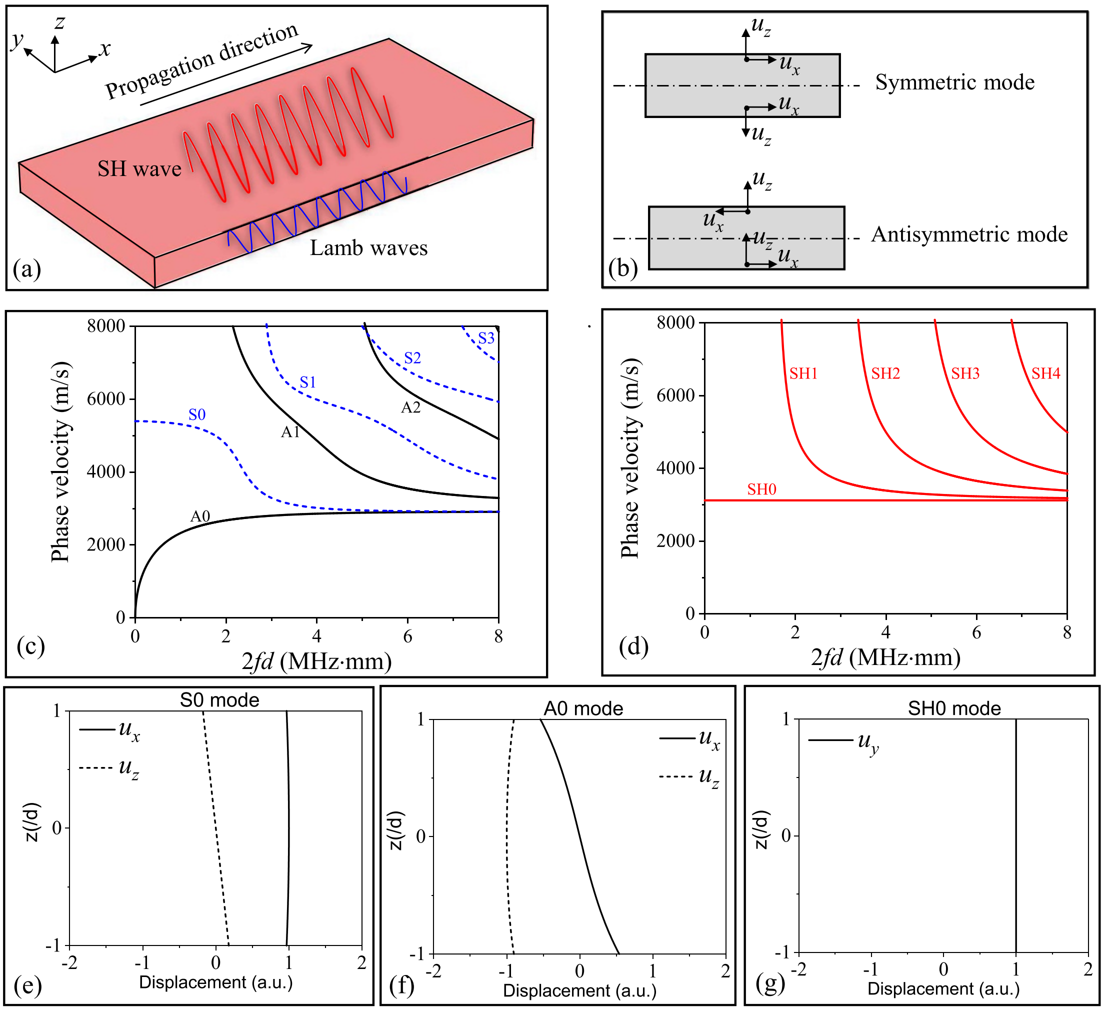

Figure 2. Guided waves in plates: (a) schematic of guided waves, (b) symmetric (S) and antisymmetric (A) modes, dispersion curves of (c) Lamb waves and (d) shear horizontal (SH) waves, and mode shapes of (e) S0 mode, (f) A0 mode and (g) SH0 mode.

in which k denotes wavenumber. Equation (1) requires $f(z)$ and $h(z)$ to have the general harmonic forms as $f(z) = A_1 \sin\eta_P z + A_2 \cos\eta_P z$ and $h(z) = B_1 \sin\eta_S z + B_2 \cos\eta_S z$, respectively, which contain unknown coefficients.

The free boundary conditions at the upper and lower surfaces result in zero stresses as,

$$T_{zz}|_{y=\pm d} = 0, \quad T_{xz}|_{y=\pm d} = 0, \tag{3}$$

where d is the half-thickness of the plate. The Cauchy stresses T_{ij} can be derived through the combination of the displacement-potential functions, geometry relations, and constitutive relations from equations (4)–(6) as

$$u_x = \frac{\partial\phi}{\partial x} + \frac{\partial\psi}{\partial z}, \quad u_z = \frac{\partial\phi}{\partial z} - \frac{\partial\psi}{\partial x}, \tag{4}$$

$$S_{ij} = \frac{u_{i,j} + u_{j,i}}{2}, \tag{5}$$

$$T_{ij} = \lambda S_{kk}\delta_{ij} + 2\mu S_{ij}, \tag{6}$$

where S_{ij} denotes the Cauchy strains.

Substituting equation (2) into equation (4) yields

$$\begin{cases} u_x = \left[(A_2 \mathrm{i}k\cos\eta_P z + B_1\eta_S\cos\eta_S z) + (A_1 \mathrm{i}k\sin\eta_P z - B_2\eta_S\sin\eta_S z)\right]\mathrm{e}^{\mathrm{i}(kx-\omega t)} \\ u_z = \left[-(A_2\eta_P\sin\eta_P z + B_1 \mathrm{i}k\sin\eta_S z) + (A_1\eta_P\cos\eta_P z - B_2 \mathrm{i}k\cos\eta_S z)\right]\mathrm{e}^{\mathrm{i}(kx-\omega t)} \end{cases} \tag{7}$$

where A_1, A_2, B_1, B_2 are four unknowns, and

$$\eta_{\mathrm{P}}^2 = \frac{\omega^2}{c_{\mathrm{P}}^2} - k^2,\ \eta_{\mathrm{S}}^2 = \frac{\omega^2}{c_{\mathrm{S}}^2} - k^2. \tag{8}$$

According to equation (7), the displacement field can be resolved into symmetric and antisymmetric components, corresponding to the respective particle motion patterns about the midplane. Substituting equation (7) into equations (5) and (6), in conjunction with the boundary condition in equation (3), the dispersion relations of S and A mode Lamb waves are obtained as follows

$$\frac{\tan\eta_{\mathrm{P}}d}{\tan\eta_{\mathrm{S}}d} = -\frac{\left(k^2-\eta_{\mathrm{S}}^2\right)^2}{4k^2\eta_{\mathrm{P}}\eta_{\mathrm{S}}}\,(\text{for Symmetric Lamb waves})\,, \tag{9}$$

$$\frac{\tan\eta_{\mathrm{P}}d}{\tan\eta_{\mathrm{S}}d} = -\frac{4k^2\eta_{\mathrm{P}}\eta_{\mathrm{S}}}{\left(k^2-\eta_{\mathrm{S}}^2\right)^2}\,(\text{for Antisymmetric Lamb waves})\,. \tag{10}$$

The above analytical solutions indicate the implicit relations between the wavenumber and frequency of Lamb waves, which can be solved numerically. As an illustration, the dispersion curves of Lamb waves in a 2 mm-thick aluminum plate (mass density of 2700 kg m^{-3}, Young's modulus of 70 GPa, and Poisson's ratio of 0.33) are plotted in figure 2(c). It can be seen that in the low-frequency region, only the lowest-order Lamb waves, including S0 mode and A0 mode, exist (under the cut-off frequencies). The two modes, however, feature distinct velocities in this low-frequency region, with the S0 mode waves travelling faster than their A0 counterparts. This feature facilitates their identification and demarcation in the time domain. In addition, the low-frequency S0 Lamb wave mode exhibits a nearly constant phase velocity and minimal dispersion. This feature has been exploited in many SHM techniques, as demonstrated in later sections.

Accordingly, the unknown coefficients (A_1, A_2, B_1, and B_2) can be calculated, and mode shapes in terms of displacements are thus obtained, as

$$\begin{cases} u_x = \mathrm{i}\left(-2k^2\eta_{\mathrm{S}}\cos(\eta_{\mathrm{S}}d)\cos(\eta_{\mathrm{P}}z) + \eta_{\mathrm{S}}\left(k^2-\eta_{\mathrm{S}}{}^2\right)\cos(\eta_{\mathrm{P}}d)\cos(\eta_{\mathrm{S}}z)\right) \\ u_z = 2k\eta_{\mathrm{P}}\eta_{\mathrm{S}}\cos(\eta_{\mathrm{S}}d)\sin(\eta_{\mathrm{P}}z) + k\left(k^2-\eta_{\mathrm{S}}{}^2\right)\cos(\eta_{\mathrm{P}}d)\sin(\eta_{\mathrm{S}}z) \end{cases}, \tag{11}$$

$$\begin{cases} u_x = \mathrm{i}\left(2k^2\eta_{\mathrm{S}}\sin(\eta_{\mathrm{S}}d)\sin(\eta_{\mathrm{P}}z) - \eta_{\mathrm{S}}\left(k^2-\eta_{\mathrm{S}}{}^2\right)\sin(\eta_{\mathrm{P}}d)\sin(\eta_{\mathrm{S}}z)\right) \\ u_z = 2k_{\mathrm{A}}\eta_{\mathrm{P}}\eta_{\mathrm{S}}\sin(\eta_{\mathrm{S}}d)\cos(\eta_{\mathrm{P}}z) + k\left(k^2-\eta_{\mathrm{S}}{}^2\right)\sin(\eta_{\mathrm{P}}d)\cos(\eta_{\mathrm{S}}z) \end{cases}, \tag{12}$$

where equations (11) and (12) correspond to S and A modes, respectively. The mode shapes of the lowest-order S and A mode Lamb waves at 300 kHz are plotted in figures 2(e) and (f), respectively, showing the polarization characteristics of both types of waves.

On the other hand, SH waves can be treated in a similar but more straightforward manner as they are y-direction polarized while propagating in the x direction. The governing equation writes

$$\frac{\partial^2 u_y}{\partial x^2} + \frac{\partial^2 u_y}{\partial z^2} = \frac{1}{c_{\mathrm{S}}^2}\ddot{u}_y, \tag{13}$$

where the displacement field of SH waves is expressed as

$$u_y = g(z)\,\mathrm{e}^{\mathrm{i}(kx-\omega t)}. \tag{14}$$

Substituting equation (14) into equation (13), the harmonic solution of $g(z)$ allows equation (14) to be expressed as

$$u_y = (C_1\,sin\,\eta z + C_2\,cos\,\eta z)\,\mathrm{e}^{\mathrm{i}(kx-\omega t)} \tag{15}$$

where C_1 and C_2 are two unknowns, and $\eta^2 = \omega^2/c_{\mathrm{S}}^2 - k^2$.

Likewise, the traction-free boundary conditions at the upper and lower surfaces are introduced, as

$$T_{zy}\big|_{z=\pm d} = 0. \tag{16}$$

Combining equations (15) and (16), in conjunction with equations (5) and (6), the characteristic equation is obtained as

$$\sin\eta d\cos\eta d = 0, \tag{17}$$

which governs the dispersion relations of SH waves. Specifically, $\cos\eta d = 0$ corresponds to the S modes, while $\sin\eta d = 0$ for A modes. The dispersion curves of SH waves, which can be solved analytically, are thus presented for the aforementioned aluminum plate in figure 2(d). The branches SH0, SH2, and SH4 correspond to the S modes, while the branches SH1 and SH3 correspond to the A modes. It can be observed that the SH0 waves are intrinsically non-dispersive. This appealing feature triggered extensive applications in both linear and nonlinear GW-SHM.

Furthermore, the mode shapes of displacements can be derived (as exemplified by the SH0 mode in figure 2(g)), as

$$u_y = C_2 \cos\eta z e^{\mathrm{i}(kx-\omega t)} \text{ (for Symmetric SH wave)}, \tag{18}$$

$$u_y = C_1 \sin\eta z e^{\mathrm{i}(kx-\omega t)} \text{ (for Antisymmetric SH wave)}. \tag{19}$$

2.2. Nonlinear GWs

The propagation of GWs in a nonlinear medium like thin-walled plates gives rise to nonlinear components, exemplified by higher harmonics, through interactions with the medium. Nonlinearities in structures can be attributed to material nonlinearity (e.g. microstructural defects) and contact acoustic nonlinearity (e.g. cracks). The analysis presented here focuses on combinational harmonics generated by two primary waves, given their prevalence in SHM applications. Notably, higher harmonic generation constitutes a special case within this broader category of combinational harmonics.

Based on the continuum mechanics theory, the material property is first retrieved by using the Green–Lagrange strain $\mathbf{E}$, which describes the nonlinear strain-displacement relation as [50, 97]

$$\mathbf{E} = \frac{1}{2}\left(\mathbf{H} + \mathbf{H}^{\mathrm{T}} + \mathbf{H}^{\mathrm{T}}\mathbf{H}\right), \tag{20}$$

where $\mathbf{H}$ is the gradient of displacement as $\mathbf{H} = \nabla\mathbf{u}$. Compared with the linear relationship described in equation (5), the additional term $\mathbf{H}^{\mathrm{T}}\mathbf{H}$ corresponds to geometric nonlinearity, which can be used to address large-deformation scenarios.

To express the nonlinear stress–strain relation of a weakly nonlinear isotropic elastic medium, a series of models based on strain energies (e.g. the Murnaghan model [98], Landau–Lifshitz model [99], Brugger model [100]) have been proposed. As an example, the Landau–Lifshitz model in a homogeneous isotropic medium is presented here, which can generally be expressed as

$$W = \frac{\lambda}{2}\left(\mathrm{tr}\left[\mathbf{E}\right]\right)^2 + \mu\mathrm{tr}\left[\mathbf{E}^2\right] + \frac{\bar{A}}{3}\mathrm{tr}\left[\mathbf{E}^3\right] + \bar{B}\mathrm{tr}\left[\mathbf{E}\right]\mathrm{tr}\left[\mathbf{E}^2\right] + \frac{\bar{C}}{3}\left(\mathrm{tr}\left[\mathbf{E}\right]\right)^3 + \cdots, \tag{21}$$

where W denotes the strain energy, the coefficients $\bar{A}$, $\bar{B}$, and $\bar{C}$ represent the third-order elastic constants which account for the generation of nonlinear waves. When omitting the higher-order terms, the second Piola–Kirchhoff stress tensor writes

$$\mathbf{T} = \lambda tr\left[\mathbf{E}\right]\mathbf{I} + 2\mu\mathbf{E} + \bar{C}(tr\left[\mathbf{E}\right])^2\mathbf{I} + \bar{B}tr\left[\mathbf{E}^2\right]\mathbf{I} + 2\bar{B}tr\left[\mathbf{E}\right]\mathbf{E} + \bar{A}\mathbf{E}^2. \tag{22}$$

According to the perturbation theory, stresses are decomposed into linear and nonlinear parts as

$$\mathbf{T} = \mathbf{T}^{\mathrm{L}} + \mathbf{T}^{\mathrm{NL}} \; with \; \mathbf{T}^{\mathrm{NL}} << \mathbf{T}^{\mathrm{L}}. \tag{23}$$

In a general case, when two waves propagate in a plate with material nonlinearity (denoted as 'a' and 'b' respectively), combinational harmonic waves can be generated, as sketched in figure 3. The nonlinear waves contain both the second harmonic due to the self-interaction of wave 'a' or wave 'b' [49, 50], and the combinational waves resulting from the mutual interaction (wave mixing) between the two primary waves [56, 57, 101]. Mathematically, the nonlinear parts of stress corresponding to the self-interaction and mutual interaction are obtained by substituting equation (20) into equation (22) as

$$\begin{aligned}\mathbf{T}^{\mathrm{NL}}_{aa(bb)} &= \bar{C}(\mathrm{tr}\left[\mathbf{H}\right])^2\mathbf{I} + \bar{B}\mathrm{tr}\left[\mathbf{H}\right]\mathbf{H}^{\mathrm{T}} + \frac{\bar{A}}{4}\mathbf{H}^{\mathrm{T}}\mathbf{H}^{\mathrm{T}} + \frac{\bar{B}}{2}\mathrm{tr}\left[\mathbf{H}^2 + \mathbf{H}^{\mathrm{T}}\mathbf{H}\right]\mathbf{I} \\ &\quad + \bar{B}\mathrm{tr}\left[\mathbf{H}\right]\mathbf{H} + \frac{\bar{A}}{4}\left(\mathbf{H}^2 + \mathbf{H}^{\mathrm{T}}\mathbf{H} + \mathbf{H}\mathbf{H}^{\mathrm{T}}\right),\end{aligned} \tag{24}$$

$$\begin{aligned}\mathbf{T}^{\mathrm{NL}}_{ab} &= 2\bar{C}tr\left[\mathbf{H}_a\right]tr\left[\mathbf{H}_b\right]I + \bar{B}\left(tr\left[\mathbf{H}_a\right]\mathbf{H}_b + tr\left[\mathbf{H}_a\right]\mathbf{H}_b^T + tr\left[\mathbf{H}_b\right]\mathbf{H}_a + tr\left[\mathbf{H}_b\right]\mathbf{H}_a^T\right) \\ &\quad + \bar{B}tr\left[\mathbf{H}_a\mathbf{H}_b + \mathbf{H}_a\mathbf{H}_b^T\right]I + \frac{\bar{A}}{4}\left(\mathbf{H}_a\mathbf{H}_b + \mathbf{H}_b\mathbf{H}_a + \mathbf{H}_a^T\mathbf{H}_b^T + \mathbf{H}_b^T\mathbf{H}_a^T\right. \\ &\quad \left. + \mathbf{H}_a\mathbf{H}_b^T + \mathbf{H}_b\mathbf{H}_a^T + \mathbf{H}_a^T\mathbf{H}_b + \mathbf{H}_b^T\mathbf{H}_a\right).\end{aligned} \tag{25}$$

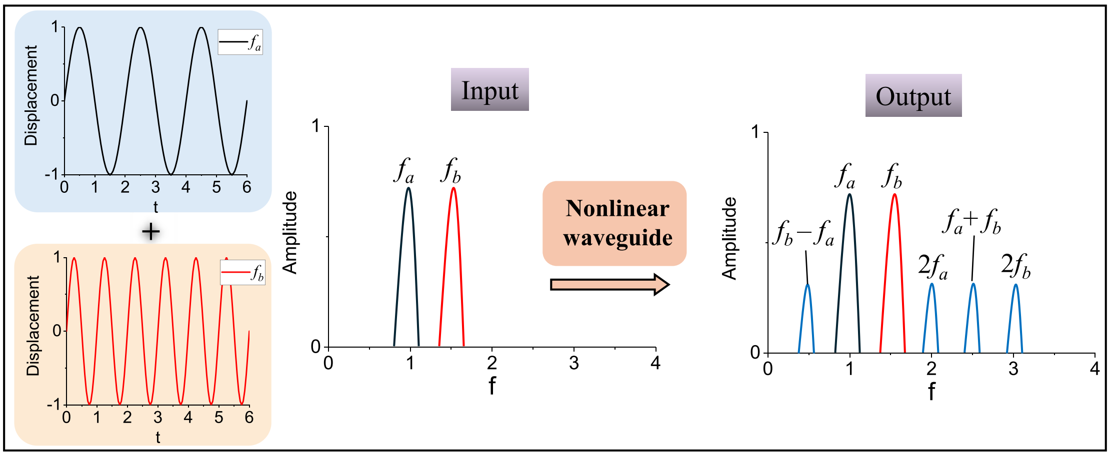

Figure 3. Schematic of nonlinear wave generation.

Note that geometric nonlinearity is omitted due to its limited contribution as demonstrated in [63, 102].

To calculate the wave field of the nonlinear components, the normal model expansion method [103] can be employed as

$$\boldsymbol{S}^{\mathrm{NL}}\left(\mathbf{u}_a,\mathbf{u}_b\right)=\frac{1}{2}\sum_{n=1}^{\infty}a_n\left(x\right)\boldsymbol{S}_n\mathrm{e}^{-\mathrm{i}\left(\omega_i+\omega_j\right)t},\left(i,j=a\text{ or }b\right),\tag{26}$$

where $\mathbf{S}^{\mathrm{NL}}$ represents the stress field of nonlinear waves, while $\boldsymbol{S}_n$ stands for the mode shape in terms of stress. a_n is the model participation coefficient, which can be calculated based on the complex reciprocity theorem as [103]

$$a_n=\begin{cases}-\frac{\mathrm{i}\left(f_n^{\mathrm{surf}}+f_n^{\mathrm{vol}}\right)}{4P_{nn}\left[k_n^*-\left(k_i+k_j\right)\right]}\left(\mathrm{e}^{\mathrm{i}k_n^*x}-\mathrm{e}^{\mathrm{i}\left(k_i+k_j\right)x}\right),\ k_n^*\neq k_i+k_j\\ \frac{\left(f_n^{\mathrm{surf}}+f_n^{\mathrm{vol}}\right)}{4P_{nn}}x\mathrm{e}^{\mathrm{i}\left(k_i+k_j\right)x},\ k_n^*=k_i+k_j\end{cases},\left(i,j=a\text{ or }b\right),\tag{27}$$

where

$$\begin{cases}f_n^{\mathrm{surf}}=-\frac{1}{2}\mathbf{T}_{ij}^{\mathrm{NL}}\mathbf{v}_n^*\cdot\boldsymbol{n}_z|_{-d}^{d}\\ f_n^{\mathrm{vol}}=\frac{1}{2}\int_{-d}^{d}\mathrm{div}\left(\mathbf{T}_{ij}^{\mathrm{NL}}\right)\cdot\mathbf{v}_n^*\mathrm{d}z\\ P_{nn}=-\frac{1}{4}\rightarrow\int_{-d}^{d}\left(\frac{\mathrm{S}_n\mathbf{v}_n^*+\mathrm{S}_n^*\mathbf{v}_n}{2}\right)\cdot\boldsymbol{n}_x\mathrm{d}z\end{cases},\left(i,j=a\text{ or }b\right)\tag{28}$$

Substituting equations (24) and (25) into equation (28), the model participation coefficient a_n in equation (27) can be calculated. With all terms in equation (26) available, the nonlinear waves can thus be obtained.

Different from the material nonlinearity, the contact acoustic nonlinearity [104] arises from structural discontinuity, such as cracks and delamination. Among various intricate mechanisms underpinning the generation of contact acoustic nonlinearity, such as hysteresis, rough surface contact, non-classical dissipation, and so on [105], the 'breathing' effect [106, 107] is regarded as the predominant cause. Under cyclic loads, the compression and tension effects of waves cause the opening and closing of cracks or delamination, generating the so-called 'breathing' behavior. The stress–strain relationship takes a distinct form during the two processes: a linear relationship persists at the closed crack, while no stress is transmitted at the open crack. The stiffness asymmetry leads to a nonlinear shear stress–strain relationship [60, 108, 109] to generate nonlinear waves. Although mathematical derivations of nonlinear waves generated by contact acoustic nonlinearity are difficult, the asymmetry in the stress–strain relation can still result in the generation of second and combinational harmonics, as illustrated in figure 3.

3. Mechanisms of metamaterials for GW manipulation

Building upon the established understanding of linear and nonlinear GWs, this section highlights the key roles of metamaterials in GW manipulation that are most pertinent to SHM. Key scenarios covered include bandgap generation, wavefront shaping, and mode customization. In addition, topological modes and non-Hermitian parity-time (PT) symmetry have also emerged recently as prominent research themes in EMs. While their integration with GW-based SHM has been less frequently reported, they show considerable promise for advanced wave control and are therefore also discussed here. Specifically, this section will focus on clarifying the fundamental mechanisms behind these phenomena and elaborating on the design principles for developing metamaterials tailored to these applications. It is worth noting that while EMs exhibit other types of extraordinary properties, only the ones closely relevant to GW-SHM, as mentioned above, are reviewed here. Other functions will not be introduced here, which have already been well reviewed in the literature, such as intelligent metamaterials [110, 111].

3.1. Bandgap generation

The bandgap constitutes a defining characteristic of EMs, representing a specific frequency range within which elastic waves are prohibited from propagating through the material. When an incident wave interacts with the specially engineered metamaterial region, it undergoes reflection or absorption, thereby preventing any energy transmission within the designed bandgap. Leveraging this, the desired GW components can be purified through filtering out other interruptive components, which is conducive to GW-SHM applications. Achieving this phenomenon necessitates the meticulous design of the metamaterial's microstructure or unit cell, along with its spatial arrangement, to induce one of the following effects: local resonance [112–116] and Bragg scattering [59, 117].

The local resonance effect serves as a pivotal mechanism for generating bandgaps in elastic wave metamaterials [68]. Such metamaterials are engineered with small-scale resonators (typically mass-spring systems) embedded in a primary matrix or attached to a host structure. Each resonator exhibits a strong intrinsic natural resonance frequency f_0. An incident elastic wave with a frequency close to f_0 propagates through the host matrix, impinges on a resonator, and excites the resonator. Notably, the excited resonator does not oscillate in phase with the incident wave. Due to inertia, the motion of the resonator's mass lags the driving force of the host matrix, leading to a 180° phase difference. In this state, the resonator mass moves opposite to the particle motion direction of the incident wave. This out-of-phase motion induces a salient phenomenon: within a narrow frequency band around f_0, the effective dynamic mass of the entire composite unit becomes negative. This negative effective mass gives rise to an extreme impedance mismatch between the sections with and without the resonator unit. Owing to this drastic mismatch, elastic waves fail to propagate through it, instead being almost entirely reflected. Since the metamaterial usually comprises a periodic array of identical resonators, the wave encounters this impenetrable barrier repeatedly, undergoing backward reflection at each resonator. Consequently, the wave amplitude decays exponentially with propagation distance, rendering the wave evanescent—i.e. it exists but does not propagate. This frequency range, characterized by exponential decay, corresponds to the locally resonant bandgap. Thus, through the rational design of resonators, the local resonance effect enables the creation of bandgaps where elastic wave propagation can be suppressed. For example, Pillarisetti *et al* [118] provided an insight into the mechanism of bandgap generation of S0-mode Lamb waves induced by local resonance. Through investigation of a classical pillar-type resonator as illustrated in figure 4(a), it was found that the bandgap is mainly determined by the resonance and antiresonance frequencies of the local resonators themselves. Accordingly, it is not necessary to consider the waveguide during the resonator design, which significantly facilitates the further topological optimization of the resonators for more advanced functions like wider bandgaps [59, 119, 120]. More recently, the inertial amplification effect [121] has been explored in conjunction with local resonance, which incorporates a geometric design of a kinematic mechanism to artificially enhance the effective inertia of the resonator. The most notable feature of the inertial amplification effect lies in its ability to generate a broad low-frequency bandgap with a compact resonator design. However, since GW-SHM usually leverages high-frequency waves (in ultrasonic scale), its relevance to SHM-specific GW manipulation is relatively limited.

Another fundamental mechanism for bandgap generation in EMs is the Bragg scattering effect [124, 125], which is essentially driven by periodic modulation. To induce Bragg scattering, a material with periodic modulation of elastic properties (density and elastic stiffness) must be constructed, which is also defined as a phononic crystal (PC). A core characteristic of such structures is the lattice constant a, referring to the distance between two identical points in the repeating unit. When an elastic wave with a

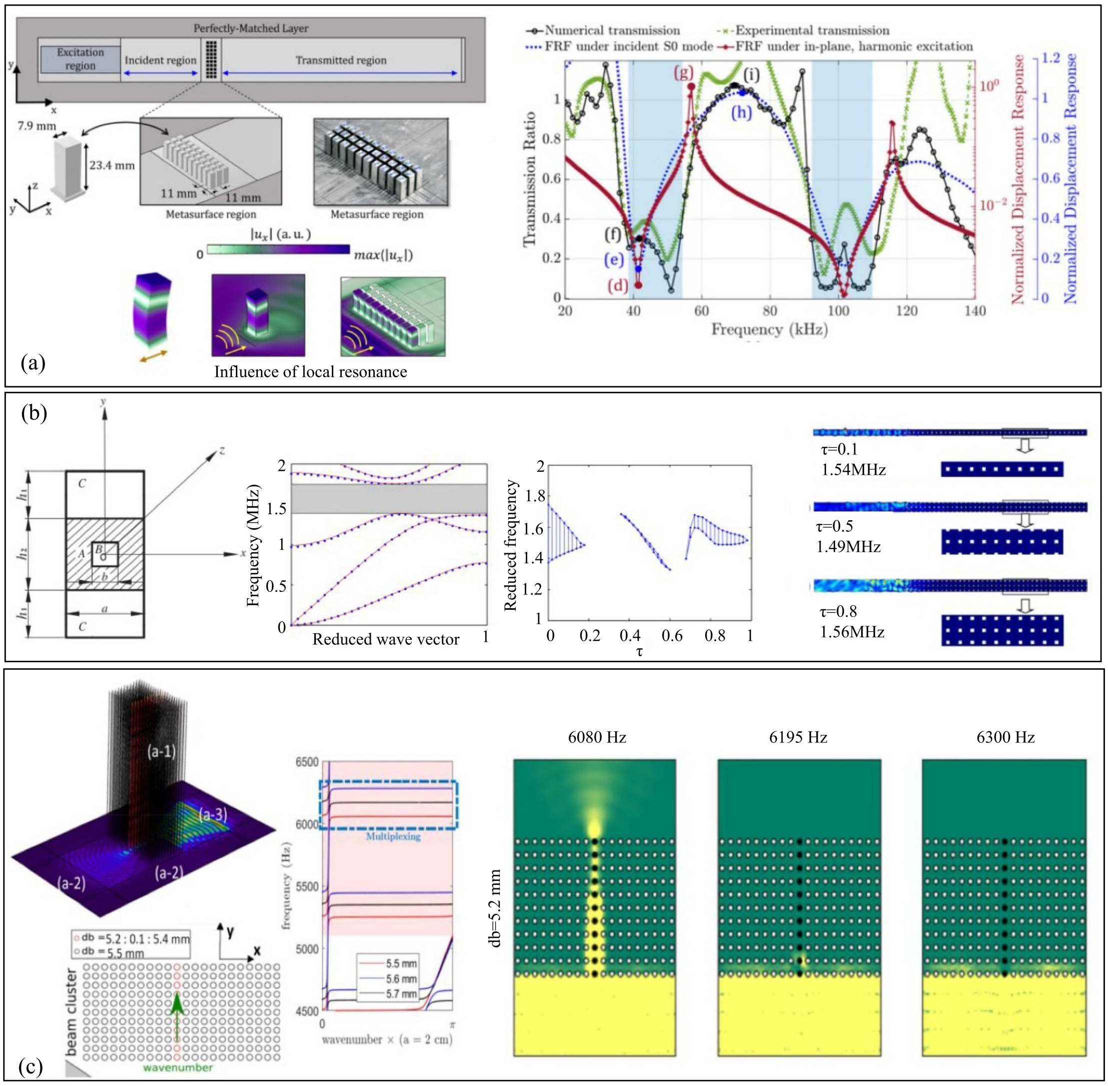

Figure 4. Mechanisms and characteristics of bandgaps of EM: (a) local resonance. Reproduced from [118]. CC BY 4.0. (b) Bragg scattering. Reprinted from [122], Copyright (2012), with permission from Elsevier. (c) Defect mode. Reproduced from [123]. CC BY 4.0.

wavelength (λ) comparable to the lattice constant propagates through this periodic structure, it interacts with periodic scatterers. According to Bragg's Law, when the wavelength approximates twice the lattice spacing ($\lambda \approx 2a$), waves undergo the most efficient backward scattering. This suppresses wave propagation through the material, leading to the generation of bandgaps in the dispersion relation. Consequently, Bragg scattering induces bandgaps at wavelengths comparable to the lattice spacing, rendering it an ideal mechanism for filtering high-frequency elastic waves. For example, Chen *et al* [122] designed a series of PC slabs to create bandgaps for Lamb waves as a result of Bragg scattering. As showcased by figure 4(b), the bandgaps can be effectively tuned for Lamb wave manipulation through varying the geometries of the unit cells.

The concept of bandgaps further gives rise to another unconventional wave phenomenon known as the 'defect' mode [126]. This phenomenon originates from the intentional introduction of a 'defect' into the well-defined periodic structure of a PC. Specifically, the incorporation of a point defect generates a highly localized state, which confines elastic wave energy at a specific frequency within the bandgap. When the configuration of defects is engineered into a linear path (i.e. a line defect [127, 128]), this localized energy can be channeled and guided along a predefined trajectory. Such a structure thereby functions as a highly efficient, frequency-selective waveguide for elastic waves. For instance, Lott *et al* [123] employed line defects to guide Lamb waves along a specific path, as illustrated in figure 4(c). By adjusting the diameter of the attached beams, the frequency of defect modes can be precisely regulated. Consequently, the metamaterial plate functions as a frequency-dependent multiplexer waveguide.

3.2. Wavefront shaping

In recent years, phononic metasurfaces incorporating two-dimensional microstructures have garnered substantial attention due to their remarkable ability to manipulate wavefronts of GWs [90, 91]. As a special type of EMs, phononic metasurface can induce a variety of anomalous wave propagation phenomena through meticulous design of its microstructures. Specifically, negative refraction [129] and reflection [130, 131] are representative scenarios where the angles of transmission or reflection can be negative relative to a positive angle of incidence, defying conventional wave behavior. In addition, metasurfaces have the capability to focus wave energy onto a specific point or partition it into multiple desired directions, thereby enabling precise control over wave propagation paths [132]. Through the employment of metasurfaces, GWs can be steered in a pre-defined manner to enhance further wave-damage interaction for GW-SHM applications.

The underlying mechanisms behind wavefront shaping are briefly recalled. When an obliquely incident wave interacts with a waveguide interface, the transmission and reflection angles (denoted as θ_t and θ_r, respectively) are governed by Snell's law, as

$$k_t \sin\theta_t = k_r \sin\theta_r = k_i \sin\theta_i. \tag{29}$$

Here, θ_i represents the incidence angle, while k denotes the wavenumber of each elastic wave component. Governed by this law, the transmitted and reflected waves propagate solely along the specific directions. However, EMs offer a paradigm shift by enabling free control over the propagation direction of GWs. For instance, they can steer GWs at angles that deviate from those predicted by Snell's law [91]. When an EM is positioned along the wave path, an incident wave can undergo oblique transmission as it traverses the metamaterial. This is achieved by spatially varying the effective elastic properties, such as density or stiffness, across the metasurface, thereby creating a gradient refractive index profile. Consequently, elastic waves bend continuously, adhering to a generalized form of Snell's law. Accordingly, a metasurface composed of subwavelength unit cells realizes artificial phase gradients perpendicular to the wave propagation direction. Let $\phi(y)$ represent the function describing the phase distribution due to the unit cells within the elastic metasurface. In this context, Snell's law can be generalized as [133]

$$k_t \sin\theta_t - k_i \sin\theta_i = k_r \sin\theta_r - k_i \sin\theta_i = \frac{\mathrm{d}\phi\,(y)}{\mathrm{d}y}. \tag{30}$$

This implies that the transmission and reflection angles can be altered by the phase gradient $\mathrm{d}\phi\,(y)/\,\mathrm{d}y$ of the metasurface. The artificially tuned phase gradient can be realized by installing unit cells that induce different phase changes [134–136]. According to the Huygens–Fresnel principle, each unit cell within the elastic metasurface can be treated as a secondary source. Consequently, the transmitted wave fields are obtained by superimposing these secondary sources. By carefully adjusting the phase of the transmitted wave through each unit cell, the desired wavefront can be formed. For example, Zhu and Semperlotti [90] proposed an elastic metasurface featuring an elliptic torus-like tapered unit cell as shown in figure 5(a). Through tuning the geometric parameters of the unit cell, its corresponding phase delays to GWs can be obtained. Besides, anomalous propagation of Lamb waves can be achieved such as deflection, focusing, and nonparaxial propagation as shown in figure 5(b). Various designs are carried out related to this topic which are comprehensively summarized in [91, 137, 138].

3.3. Mode conversion

Another crucial function of EMs is mode conversion [139–141], which enables the transfer of wave energy between different modes. As mentioned earlier, different GW modes exhibit varying sensitivities to different types of defects in GW-SHM. Thus, for detecting specific defects, converting other GW modes (which are inevitably excited in the structure) into the target mode offers significant advantages.

EMs with anisotropic characteristics, wherein effective stiffness or density varies with direction, can induce mode conversion by regulating the polarization state of GWs. The underlying mechanism is as follows: in an ideal infinite isotropic medium, GW modes are decoupled and propagate independently. Through introducing an anisotropic unit cell (either embedded in or surface-attached to the host structure), its mechanical properties, primarily in terms of the elastic stiffnesses, exhibit direction-dependent variations. When an incident wave impinges on this anisotropic unit cell, asymmetric force responses are generated, leading to complex direction-dependent oscillations [142, 143]. This asymmetrically oscillating unit cell then re-radiates (scatters) energy in all directions. Although a single unit cell only induces weak localized conversion, arranging these cells in a periodic array to form a PC or metamaterial enhances the

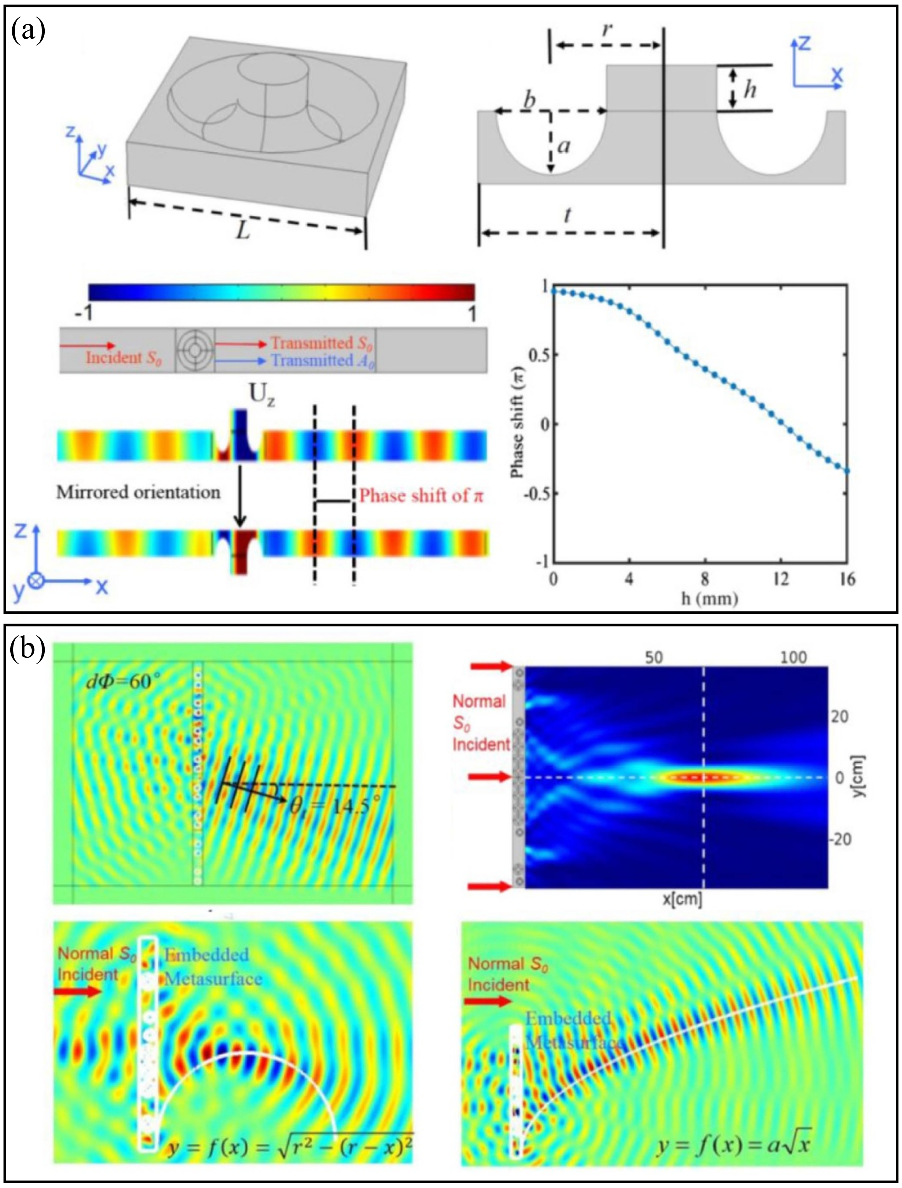

Figure 5. Mechanisms and characteristics of wavefront shaping: (a) the phase modulation mechanism and (b) propagation direction customizations. Reprinted (figure) with permission from [90], Copyright (2016) by the American Physical Society.

conversion effect to a significant and designable level. For example, Kweun *et al* [142] leveraged a transmodal Fabry-Pérot resonance mechanism to convert an S0-mode Lamb wave to an SH0-mode wave, as shown in figure 6(a). The designed metamaterial essentially introduces material anisotropy to couple the two guide wave modes. In addition, the metamaterial can also allow a reciprocal conversion from an SH0 mode to an S0 mode. Side-coupled pillared resonators and composite PC plates have been utilized for this purpose. In another case in figure 6(b), Ding *et al* [144] proposed a composite PC plate with antisymmetric and symmetric cells to achieve an efficient conversion from A0 to S0 mode Lamb waves.

3.4. Topological modes

The concept of topological modes originates from the field of condensed matter physics and has been further extended to the study of elastic waves [145, 146]. Through the precise design of EMs, topological insulators can be constructed, wherein waves are prohibited from propagating within the bulk of the material but can propagate stably along the interfaces or edges. Leveraging this property, GWs in topological modes enable unidirectional propagation along a predefined path and exhibit immunity to backscattering [147, 148], thus demonstrating unprecedented robustness against structural imperfections. This characteristic holds significant potential for integration into GW-SHM systems, particularly for damage detection along specific paths, as it can enhance the signal-to-noise ratio of detection signals.

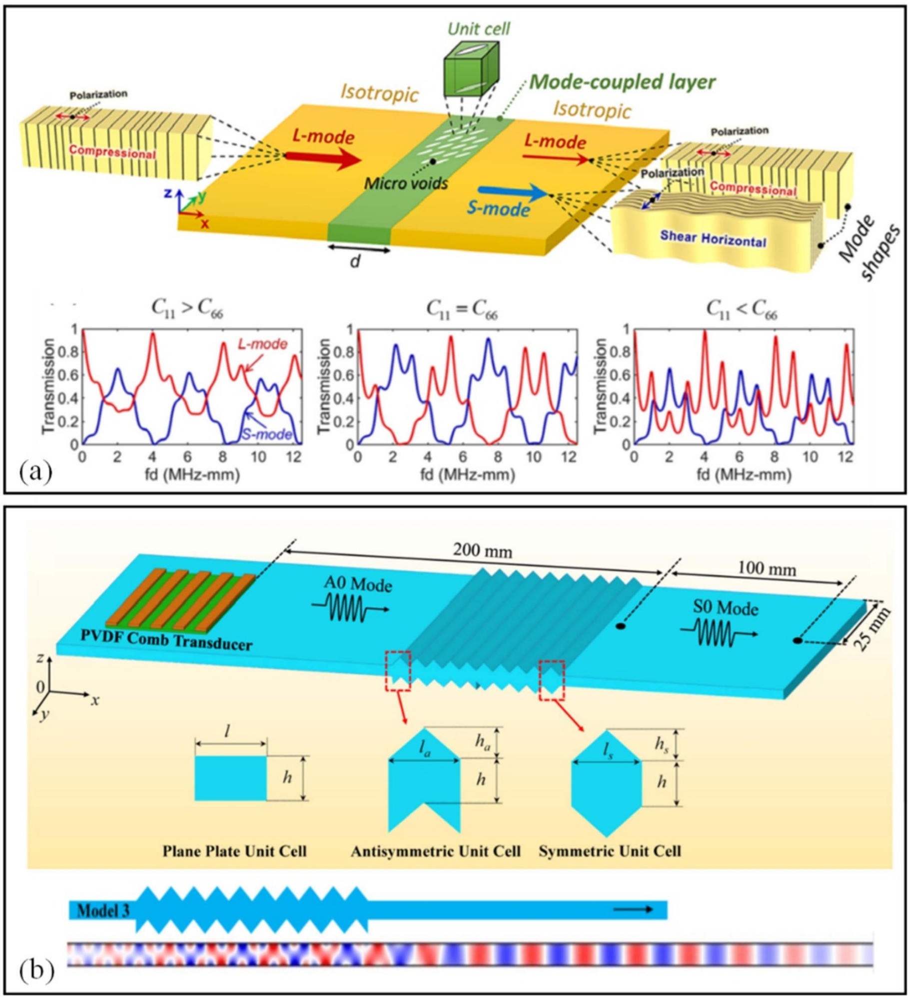

Figure 6. Examples of guided wave mode conversion: (a) from S0 mode to SH0 mode. Reprinted (figure) with permission from [142], Copyright (2017) by the American Physical Society. and (b) from A0 mode to S0 mode. Reprinted from [144], with the permission of AIP Publishing.

The design of topological metamaterials is centered on generating topological modes, a process that typically relies on the construction of two distinct topological phases [149]. Specifically, two sets of periodic structures are designed: while these structures may share similarities in geometric morphology, their band structures differ significantly in terms of topological invariants (e.g. Chern number [150], valley Chern number [151], or Zak phase [152]). This distinction gives rise to a paired system consisting of a topologically trivial structure and a topologically non-trivial structure. According to the bulk-boundary correspondence principle, when two materials with different topological invariants are arranged adjacently, a unique interface state inevitably emerges within their common bandgap. When an external excitation source generates waves within the bandgap of the bulk materials, such waves cannot propagate through the bulk of either material and instead behave as evanescent waves with exponential decay. However, guided by the bulk-boundary correspondence principle, the wave energy does not simply dissipate; instead, it is perfectly localized at the interface between the topologically trivial and non-trivial regions. This phenomenon defines the ‘waveguide,’ with the interface itself serving as the guiding channel for the wave. The most prominent feature of topological modes is their robustness: if defects (e.g. missing unit cells) exist along the GW path, the wave will not undergo backscattering toward the excitation source. Even when encountering 90° bends or sharper angular deviations in the path, the wave can propagate without losses caused by back-reflection. As long as the global topological order of the system remains intact, random imperfections in the structure will not impede wave propagation. The underlying mechanism for this behavior lies in the topological protection of the forward-propagating mode within the topological waveguide. States that can induce backscattering are topologically forbidden due to their association with a different topological phase. Coupling between these states and the propagating mode would require a drastic alteration to the global topological structure of the system,

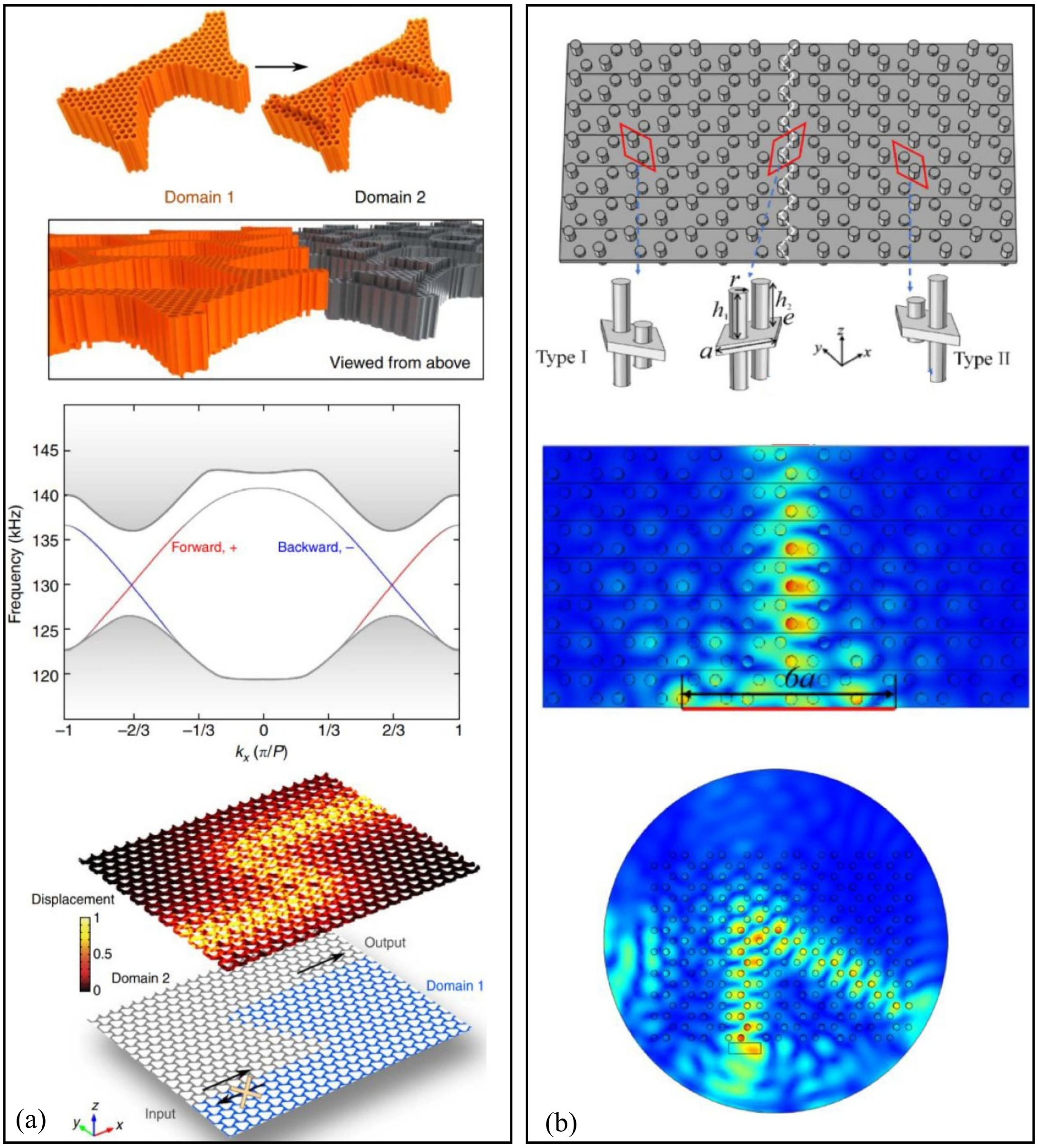

Figure 7. Realization of topological modes through (a) perforated lattice design. Reproduced from [145]. CC BY 4.0. and (b) add-on lattice design. Reproduced from [147], with permission from Springer Nature.

which cannot be achieved by local defects. For example, Mousavi *et al* [145] proposed a dual-scale PC slab to realize a strong spin-orbit coupling breaking spatial mirror symmetry, as shown in figure 7(a). Consequently, phononic edge states are generated which show significant robustness against scattering from discrete defects as well as disorders in the continuum. Chen and Nie [147] designed a hexagonal lattice PC plate by changing the spatial symmetry of the unit cell for the generation of the edge state in figure 7(b). Results show that both zigzag-type edge and bridge edge are topologically protected only for the A0 mode Lamb wave but not for the S0 mode.

3.5. Non-Hermitian PT symmetry

In the literature, most EMs tailored for wave manipulation belong to Hermitian systems, where the control of GW propagation has primarily relied on modulating the real parts of elastic constants or other material parameters. However, a burgeoning frontier has shifted focus to EMs operating as non-Hermitian systems [153]: non-conservative open systems characterized by energy loss and/or gain arising from environmental interactions. In such open systems, GWs can be manipulated by tuning the gain-and-loss factor. Through precise adjustment of gain/loss, non-Hermitian PT symmetry holds great potential for advancing GW-SHM from two key perspectives: (1) it enables non-reciprocal GW propagation [154], which can enhance wave-damage interactions while suppressing unwanted reflections; (2) it induces an exceptional point (EP) [155] in the band structure, an entity exhibiting extreme sensitivity to structural perturbations, thereby facilitating the detection of micro-defects.

The propagation behavior of GWs in this system is governed by the gain/loss coefficient and the coupling strength between gain and loss regions. When gain and loss are relatively weak compared to the coupling strength, the system resides in the exact PT-symmetric phase. Here, the guided modes possess real wavenumbers, indicating wave propagation without exponential growth or decay. In that case, despite the overall structural symmetry, wave energy becomes predominantly localized in the gain region. This phase endows the non-reciprocal GW propagation in such material. This phenomenon arises because reflected waves from the gain and loss segments undergo destructive interference for one incidence direction and constructive interference for the other. When the gain/loss strength exceeds a critical threshold, the system undergoes a phase transition to the broken PT-symmetric phase. In this phase, GW modes exhibit complex propagation wavenumbers. Consequently, one mode experiences exponential growth (gain-dominated) while the other undergoes exponential decay (loss-dominated). The transition between the exact and broken phases occurs at the EP, a singularity with unique physical properties. At the EP, the two formerly orthogonal guided modes coalesce into a single mode, with their eigenvalues and eigenvectors becoming identical. This coalescence renders the system exquisitely sensitive to tiny perturbations: an infinitesimal environmental change (e.g. a minor mass reduction, slight fluctuations in temperature or pressure) triggers a significant, measurable shift in the output responses. For example, Rosa *et al* [155] investigated EPs of elastic waves in continuous media by enforcing PT symmetry through tailored balanced gain and loss, as shown in figure 8(a). It was demonstrated that the introduction of external perturbations leads to a splitting of the eigenvalues, making the EP an extremely sensitive approach to the detection of such perturbations as added masses, stiffness discontinuities, and surface cracks. In addition, Yi *et al* [156] proposed a tunable and reconfigurable non-Hermitian piezoelectric metamaterial bar, in which piezoelectric bars connect with resonant circuits as illustrated in figure 8(b). It achieves non-reciprocal wave propagation, which is further used for asymmetric unidirectional and symmetric bidirectional perfect absorption of elastic waves.

4. SHM-specific metamaterial design and applications

While EMs can enable a wide range of remarkable wave phenomena, research remains predominantly focused on mechanism exploration and phenomenon demonstration. Studies of their engineering applications are still limited, particularly in the field of SHM. SHM applications impose harsh and unique requirements on EM design and deployment. In particular, structural integrity must be preserved, which restricts the use of existing perforated metamaterial designs. Instead, EM material/devices should be designed as an add-on component to the existing structure under inspection. As such, many of the existing studies mentioned above, focusing on the design of materials through which elastic energy entirely passes, cannot be directly used. The designed materials are rather considered as add-on devices to indirectly interact with the elastic waves inside the waveguide. This inevitably increased difficulty in designing the meta-device and achieving the expected wave manipulation outcome. Accordingly, this section reviews current research on guided-wave manipulation using attached structures. Following the typical stages in an SHM system, the discussion is organized into wave generation, propagation, and sensing. Finally, representative SHM application cases are presented to showcase how metamaterials can enhance SHM performance.

4.1. Modulated GW generation

(1) **Wave purification.** In practice, the complexity of the measurement system gives rise to higher harmonic energy generated by the nonlinearities in equipment, transducers, and adhesive bonding layers when actuating/sensing elements like PZT are used. These harmonics distort the acquired GW signals and hinder the accurate extraction of damage-related information. This issue becomes particularly critical in nonlinear-guided-wave-based SHM, where higher harmonics originating from non-damage-related sources can obscure or overwhelm the damage-induced nonlinear components. As a result, such interference may dominate the measured signals and compromise the effectiveness of SHM techniques. To address this issue, the concept of metamaterials is embraced to develop selective wave filters dedicated to SHM applications, as schematized in figure 9(a) [157]. Along this line of thinking, Ciampa *et al* [158] designed an ultrasonic PC waveguide transducer, where corrugation structures are deployed on the host structure surrounding a transducer. The phononic structures were designed with desired bandgaps in the second harmonic frequency region of the excitation

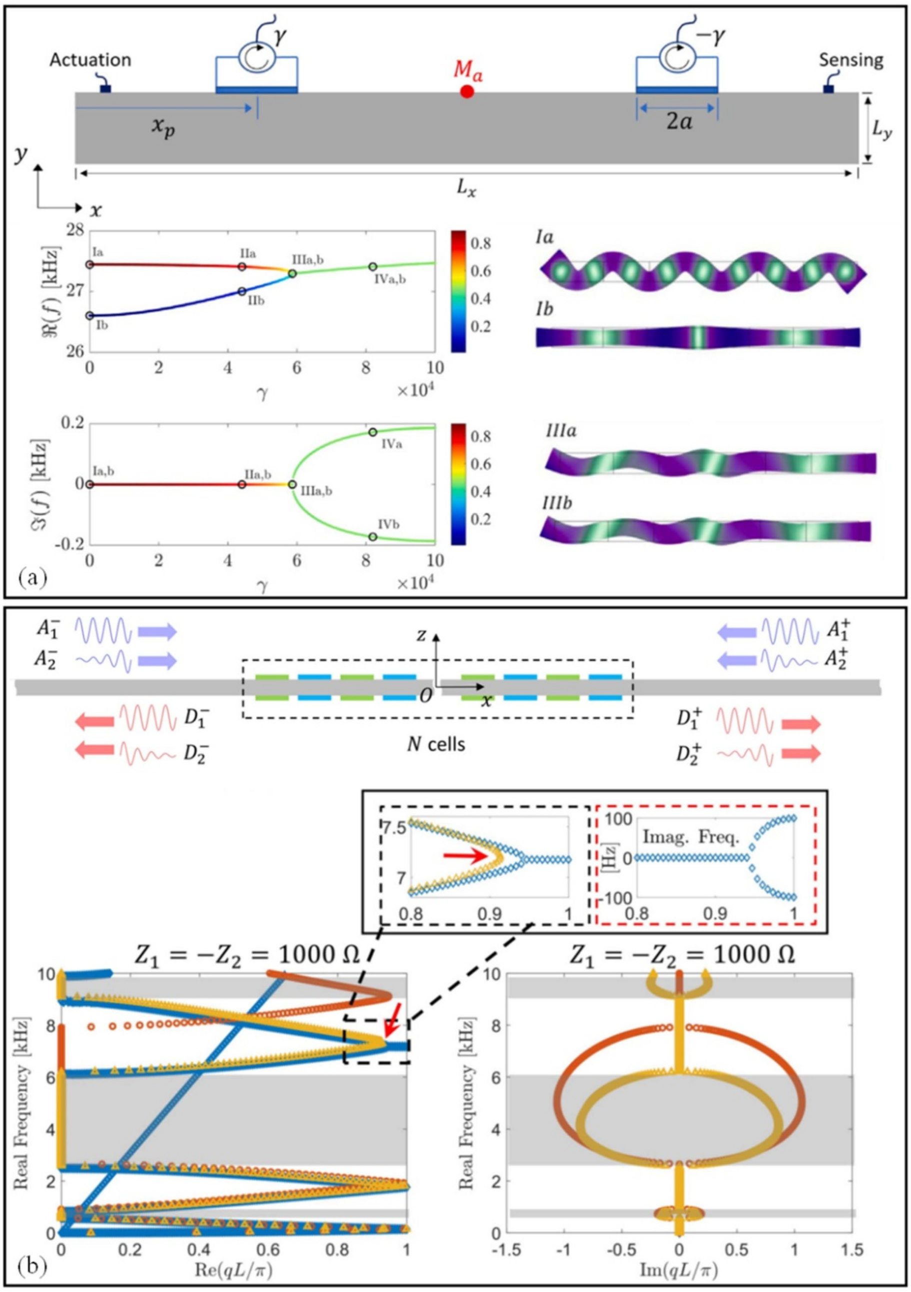

Figure 8. (a) Characteristics of an exceptional point. Reprinted from [155], Copyright (2021), with permission from Elsevier. and (b) realization of an exceptional point through piezoelectric circuits. Reprinted (figure) with permission from [156], Copyright (2022) by the American Physical Society.

frequency to filter fictitious nonlinear components generated at the trigger part. Tian *et al* [159] developed a composite metamaterial with cylinders to mitigate the undesired nonlinearity, as shown in figure 9(b). The metamaterial structures are attached to the surface of the host structure to maintain structural integrity. Liu *et al* [157] proposed a topologically designed metamaterial filter to achieve broadband elimination of the deceptive second harmonic waves, as shown in figure 9(c). Upon tactically introducing deceptive nonlinear sources such as the nonlinear adhesive bonding layers in a piezoelectric transducer-activated SHM system, the performance of the meta-filter was examined from the SHM perspective. Similar studies considering different metamaterial configurations, host structures under inspection, and damage types used for function validation have also been reported in recent literature [160–165], as exemplified in figure 9(d).

(2) **Directional emission.** As an important function in SHM, the directional GW generation ability is required in some applications to achieve directional scanning and inspection of structures. While the phased array technique can achieve directional wave generation, it requires multiple physical channels

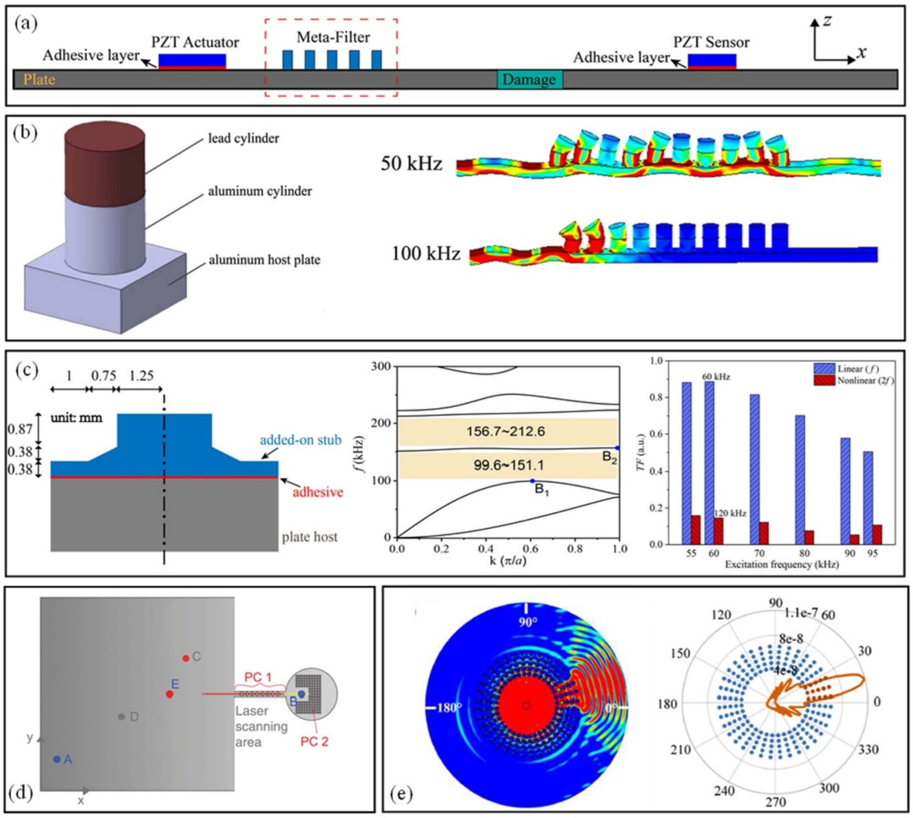

Figure 9. (a) Schematic of meta-filter-assisted damage detection. Reproduced with permission from [157]. (b)–(d) several metamaterial designs using different configurations for simultaneously passing fundamental waves and suppressing secondary waves. (b) Reproduced from [159]. © IOP Publishing Ltd All rights reserved. (c) Reproduced with permission from [157]. (d) Reprinted (figure) with permission from [165], Copyright (2022) by the American Physical Society. (e) directional wave emission using a metasurface radar. Reprinted from [166], Copyright (2023), with permission from Elsevier.

with associated transducers, resulting in increased cost and system complexity. To address this issue, metamaterials can be designed to guide the direction of wave generation with only a single actuator. For example, Song and Shen [166] proposed a metasurface radar made of shape memory alloy (SMA) unit cells for wave generation in designated directions. Through controlling the geometry of SMA, the bandgap can be tuned so that the wave emission directions can be manually controlled, as shown in figure 9(e).

4.2. Customized wave propagation

(1) **Selective mode transmission.** In SHM applications, the foremost requirement for GW generation is to excite clean and strong waves at target frequencies. However, as discussed in section 2, the multi-mode feature of GWs compromises their use in SHM due to the increased signal complexity, which makes the identification of useful damage information difficult. Besides, the sensitivity of different GW modes to a specific type of damage varies. Therefore, add-on metamaterials can be designed to enhance the desired modes and suppress others. For example, EMs enable the selective passing of different GW modes through engineering band structures. At the targeted frequency, the mode shape only exhibits the displacement pattern of a single mode, including S mode, A mode, or SH mode. For example, Liu *et al* [59] customized broad passing frequency bands, where only the S0 or A0 mode Lamb waves can pass while the other one is filtered out, using topologically designed and surface-mounted meta-devices, as illustrated in figure 10(a). The selective passing feature of the meta-device at the frequency band is revealed by the anisotropy property characterized by dynamic effective material parameters, which was further validated using a finite number of unit cells in FE simulations and experiments. Other configurations of metamaterials have also been used to achieve this [167]. Xia *et al* [168] achieved S0 mode transmission within an A-mode bandgap using metamaterial filters composed of a periodic PZT array, as shown in figure 10(b). Tian and Shen [169] employed double-sided composite metamaterials to achieve single-mode bandgaps, thereby enabling selective mode transmission. Using the metamaterials, the undesired waves are reduced. Ma *et al*

[58] employed metamaterials to suppress the dispersion of GWs by tuning the effective material properties. Cao *et al* [170] leveraged the fact that SH waves can pass through curved surfaces with low reflection to filter Lamb waves for pure SH wave generation. In addition, waves propagating in pipe-like structures have also been manipulated based on the similar principle [171].

(2) **Mode conversion.** In addition to selective mode transmission, wave mode can also be customized based on mode conversion for the detection of a specific type of damage. Liu *et al* [172] designed topology-optimized metamaterials to maximally convert A0 mode Lamb waves into S0 mode Lamb waves because the latter in the low-frequency region can better satisfy the phase group matching condition, resulting in cumulative second harmonics, which facilitate the monitoring of distributed large-area damage. The capacity of the designed metamaterial converter is demonstrated by both linear and nonlinear responses. Furthermore, targeting SH waves used in SHM applications, an SH wave generation scheme is proposed based on the mode conversion from Lamb waves activated by piezoelectric transducers [144, 173, 174], as exemplified in figures 10(c) and (d). A metamaterial-mediated converter, mounted on the surface of a host structure, is designed to achieve high-efficiency energy conversion from Lamb waves to SH waves. Experimental results by Liu *et al* [173] demonstrated that the amplitude of SH waves can be increased significantly from 15 mV to 155 mV with the aid of the meta-converter, as illustrated in figure 10(c), evidencing its efficacy for SH wave generation. The method paves a novel way for further SH-wave-based SHM applications [31, 175, 176].

(3) **Wave beam steering.** GWs generated by transducers propagate with fixed patterns, characterized by wave amplitude, mode, and propagation direction. Apart from the amplitude and mode, wave propagation direction can also affect the detection capacity for specific areas of interest. However, traditional techniques mainly rely on the use of sensor arrays, which employ multiple transducers to achieve wave beam forming. This is not convenient to implement in engineering practice due to the increased installation complexity. To address this issue, the concept of metamaterials can be introduced to achieve flexible control of probing waves through wave steering. This results in the design of the so-called meta-lens, which are essentially the phase-gradient metasurfaces. When the excited waves pass through the meta-lens, the refracted waves can be tactically steered with desired energy flow patterns by designing corresponding elements with specific phase delay in sequence. This can facilitate the monitoring of a specific direction or zone of the structure. For example, Liu *et al* [101] employed the surface-mounted metasurface to simultaneously control the refracted S and A mode Lamb waves, as shown in figure 10(e), so as to convert the incident cylindrical waves into planar waves. With the assistance of the metasurface, the mixing of the fundamental S and A mode waves is enhanced, resulting in the generation of stronger second harmonic A0 waves.

(4) **Boundary reflection manipulation.** In GW-SHM, boundary reflection constitutes a critical factor influencing system performance. In most scenarios, it is necessary to suppress these reflections to prevent interference with the direct-arrival waves in order to expand the inspection area. This requirement is particularly critical for linear GW techniques that rely on precise arrival time measurements. To address this, metasurfaces can be implemented on structural boundaries. Thereby, the reflected waves are scattered and effectively decoupled from the original sensing path, preventing their reception by the sensor. For example, Hu *et al* [177] deployed thickness-gradient structures on the boundaries to mitigate GW echo, as sketched in figure 10(f). Experiments confirm that the printed samples can help to reduce reflected waves at the received signals. Nevertheless, in certain applications, the boundary reflection can in turn facilitate the extraction of damage information. For example, the coda wave interferometry (CWI) technique highly relies on the structural boundaries to facilitate wave-damage interactions. To enhance the sensitivity of CWI, Shan *et al* [178, 179] leveraged the metamaterials as artificial boundaries to increase boundary reflection paths, as shown in figure 10(g). With the installation of the artificial boundaries, the probing waves are better confined within the inspection zone. As a result, damage information can be accumulated and intensified, facilitating its identification.

4.3. Dedicated wave sensing

(1) **Wave filtering.** Before being captured by the sensor, the propagating GWs may contain tedious information, including multiple mode and frequency components. These mixed components are hard to distinguish and may even mask the damage-related components of interest. For instance, in nonlinear GW-SHM using second harmonic S0 mode waves, it is ideal that only the specific

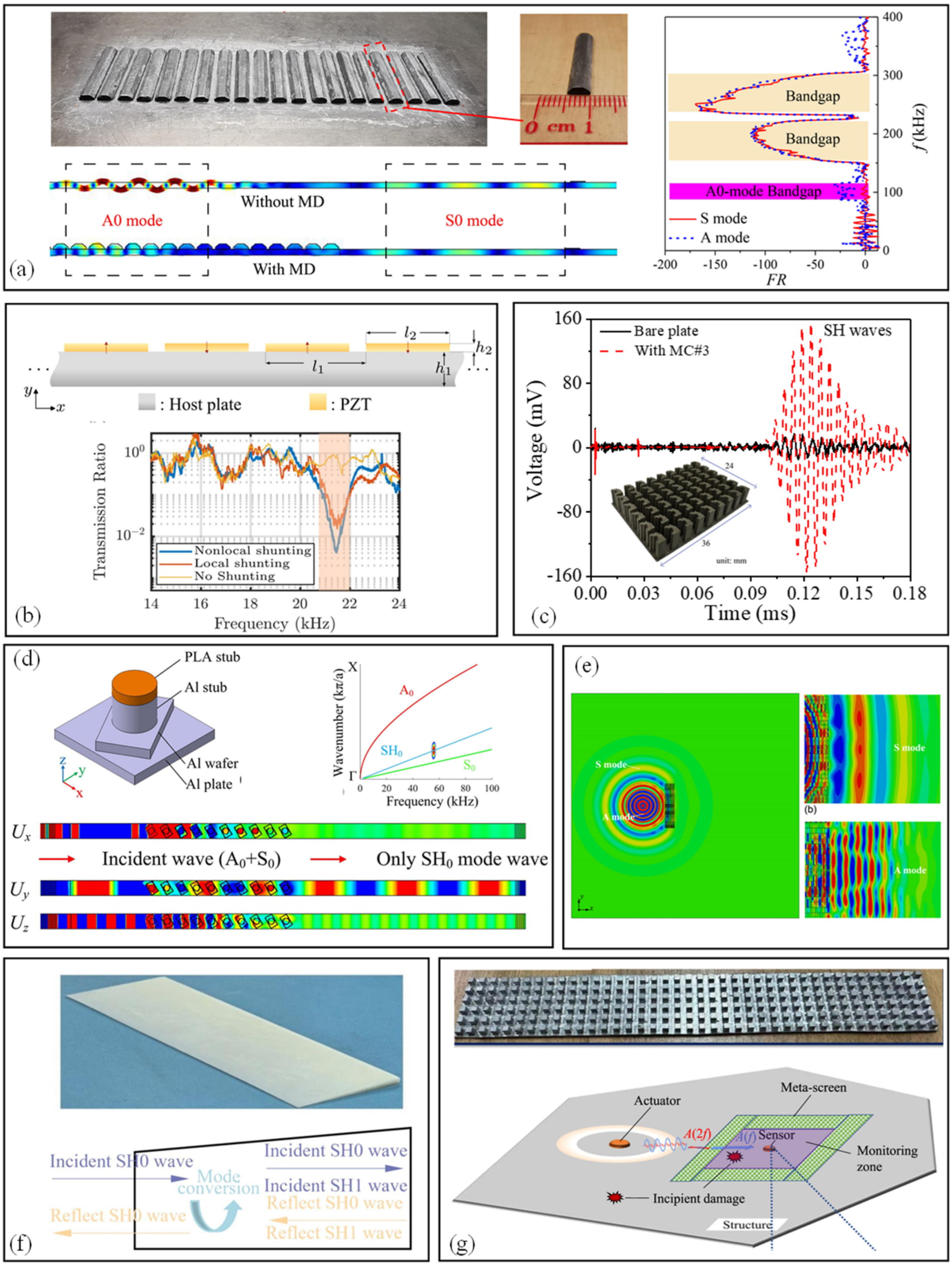

Figure 10. (a) and (b) Selective S or A mode transmission. (a) Reproduced from [59]. © IOP Publishing Ltd All rights reserved. (b) Reprinted from [168], with the permission of AIP Publishing. (c) and (d) Mode conversion between different guided waves. (c) Reprinted from [173], Copyright (2024), with permission from Elsevier. (d) Reprinted from [174], Copyright (2025), with permission from Elsevier. and (e)–(g) propagation direction manipulation, such as wave steering and reflection control. Reproduced from [101]. CC BY 4.0. Reprinted from [177], Copyright (2025), with permission from Elsevier. Reproduced from [179]. © IOP Publishing Ltd All rights reserved.

component is captured for damage diagnosis. However, the practical captured signals may contain fundamental-frequency components, second harmonic A0 mode waves, and other higher harmonics. To address this issue, metamaterials can be designed to be installed at the sensing end. For example, Kudela *et al* [180] employed a metamaterial filter to suppress the fundamental waves and simultaneously maintain the harmonic waves for easier extraction of damage information, which may simplify the signal post-processing, as shown in figure 11(a).

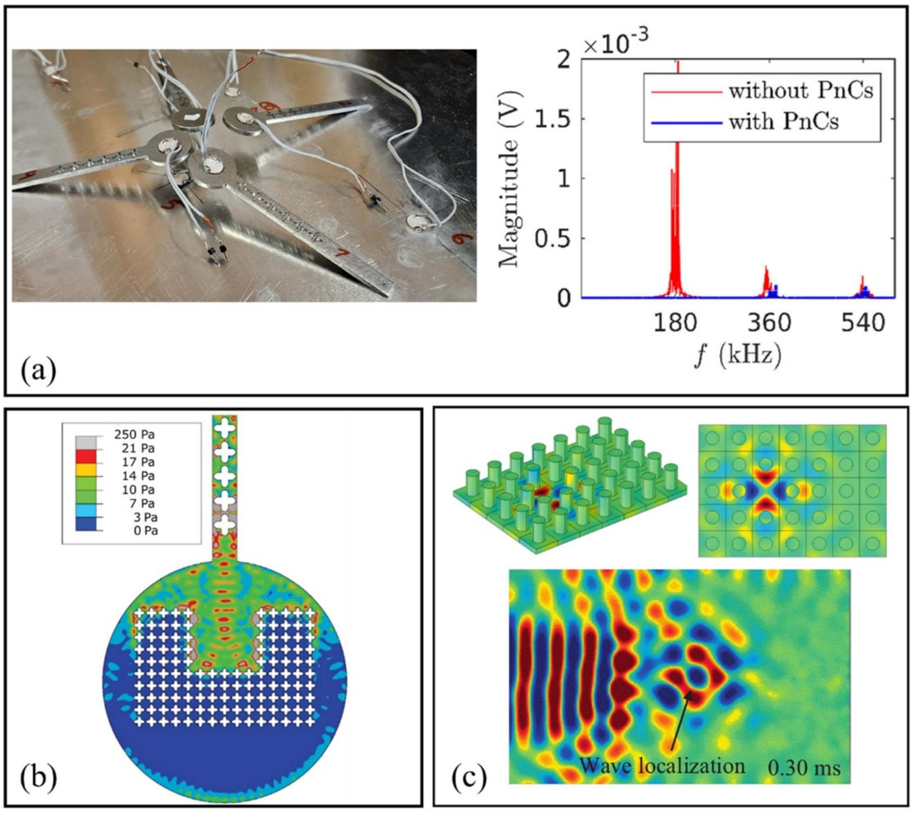

Figure 11. (a) Wave filtering. Reprinted from [180], Copyright (2026), with permission from Elsevier. (b, c) energy trapping. (b) Reprinted (figure) with permission from [165], Copyright (2017) by the American Physical Society. (c) Reprinted from [181], Copyright (2026), with permission from Elsevier.

(2) **Energy trapping.** Damage-induced GW components can be relatively weak or be overwhelmed by environmental noise, which calls for the effective extraction of damage signal. This challenge can be more severe in nonlinear GW-SHM methods where the higher harmonic waves are extremely weak. To enhance the intensity of the received waves, a possible approach is to focus wave energy and then capture it by a sensor at the focusing location. Metamaterials offer an effective means for wave focusing based on certain functions [165, 181, 182]. Specifically, with the aid of metamaterials, the propagating waves will be manipulated and trapped in the sensor position. For example, Miniaci *et al* [165] developed a C-shaped PC array composed of perforated unit cells around the sensor. Due to the bandgap effect, waves are reflected by the PCs, and the harmonic waves induced by nonlinear elasticity are enhanced, as illustrated in figure 11(b). Tian *et al* [183] utilized the rainbow trapping phenomenon delivered by a series of gradient cylinders to enhance received waves. Through a proper selection of the excitation frequency, the wave energy is focused at a desired location and then captured by the sensor. Furthermore, the defect mode phenomenon of metamaterials is employed to achieve energy trapping in the sensing end, as proven in figure 11(c) [181].

(3) **Directional sensing.** Similar to directional wave generation, wave sensing at specific directions is also important in some applications. This allows for discerning the direction of incident waves, therefore facilitating damage localization in SHM with a simple system. In this context, the same design principle of EMs in the directional emission case can be applied to the sensing end for directional sensing [184].

4.4. Enhanced SHM applications

The EMs developed above have demonstrated their effectiveness in achieving various wave manipulation functions critical for SHM. Accordingly, the following discussion will focus on integrating these EMs into practical damage detection frameworks, examining their application in the context of both linear and nonlinear GW-SHM methodologies.

(1) **Linear GW-SHM applications.** Monitoring of damage/defects with the assistance of metamaterials has been explored in linear GW SHM applications. For example, CWI was enhanced by artificial boundaries composed of customized metamaterial filters [178], as shown in figure 12(a). The metamaterial boundaries enhance the reflection of GWs, facilitating the accumulation of weak damage information in coda waves. Results confirm that the meta-devices significantly improve the coda wave-based detection method for the monitoring of a 0.2 mm-thick notch. In addition, through different combinations of metamaterial filters, zone-by-zone damage localization was achieved using selected excitation frequencies. Cao *et al* [184] developed a metamaterial-surrounded transducer to identify the orientation of scattered waves induced by damage, which was realized using surface-attached cylindrical magnets with a diameter of 10 mm. Through customizing the dispersion properties of each local resonance metamaterials, damage identification was achieved using a single receiver.

(2) **Nonlinear GW-SHM applications.** As mentioned above, there exist two main challenges in nonlinear GW-SHM: the interference from non-damage-related sources and the weak nature of nonlinear waves.

The interference from non-damage-related sources can be mitigated by developing proper metamaterial filters, which can suppress the second harmonic waves while passing fundamental waves, as mentioned in section 4.1. Based on this concept, the applications of meta-filters for damage detection have been investigated. For example, Gao *et al* [164] achieved the monitoring of corrosion damage, created by wetting the tissue with hydrochloric acid solution, on circular tubes, as shown in figure 12(b). Shan *et al* [160] applied the second harmonic S0 mode Lamb waves purified by meta-filters to inspect thermal aging-induced material degradation distributed in a 100 mm-long heating zone (in figure 12(c)). Results confirm the improved monitoring sensitivity to material microstructural changes created by heating, demonstrating the feasibility of the technique in SHM applications. Meanwhile, Liu *et al* [157] improved the capability of meta-filters for enabling broader band operation frequencies, covering 100–200 kHz frequency band commonly used in nonlinear GW-SHM. By using the designed filter on a metallic beam subject to bending, the plasticity damage evolution at different deformation stages, created by increasing (from 1 to 4) bending cycles, is characterized successfully, evidenced by visible damage-related signal variation, as shown in figure 12(d). Tian *et al* [159] achieved the detection of notch-induced fatigue damage using composite metamaterial filters. The size of the fatigue crack develops from 0 mm to 4 mm, corresponding to increasing intensity of second harmonic waves. This variation was identified owing to the reduced threshold of nonlinear waves purified by metamaterials. Sherwood *et al* [161] designed a corrugated PC waveguide for three-dimensional wave filtering. A 1 mm-long incipient crack was detected using the metamaterial-assisted SHM method. Aslam *et al* [163] successfully identified and localized CAN-related damage generated by PZT debonding, after filtering the actuation-related harmonics.

The weak nonlinear waves can be enhanced by manipulating the mode, propagation direction and energy distribution of probing waves as described in sections 4.2 and 4.3. With the deployment of the EMs, the sensitivity of existing nonlinear GW-SHM methods to incipient damage can be significantly improved. For example, the metamaterial-enabled intentional mode conversion from A mode to S mode was shown to enhance the generation of cumulative second S mode waves [172], as shown in figure 12(e). The fundamental S mode waves were increased by 60%, with their second harmonic counterparts augmented by 255%. Thermal aging damage, as a representative distributed incipient damage, was induced by surface-attaching a 10 cm × 10 cm heating block to the host structure for three hours. The signal variation of the second S mode waves became more pronounced owing to the use of the A–S meta-converter. The metamaterial-enhanced CWI can also be extended into nonlinear GW-SHM [179]. Metamaterial boundaries allow the passing of fundamental waves while stopping the second harmonics generated from outer interfering sources. A thermal aging treatment at 60 °C was applied to two surface-affixed 30 mm × 30 mm patches, which were respectively deployed on the inner and outer metamaterial zone, for one hour. The local thermal aging damage information inside the meta-screen was then accumulated within this zone and became more readily observable in the captured code waves, whilst the outer damage having much less impact. Moving to the sensing part, the detection of fatigue crack damage can be enhanced by intentionally localizing the damage information around the sensor location. The defect mode-induced energy localization [181] has been proposed using the concept of metamaterials. Results confirm the amplified received signal containing fatigue crack-induced (from 0 to 10 mm) nonlinear components, as illustrated by the results shown in figure 12(f). The 6.3 times improvement of damage index enabled by the metamaterial indicates the applicability of the proposed technique for damage detection.

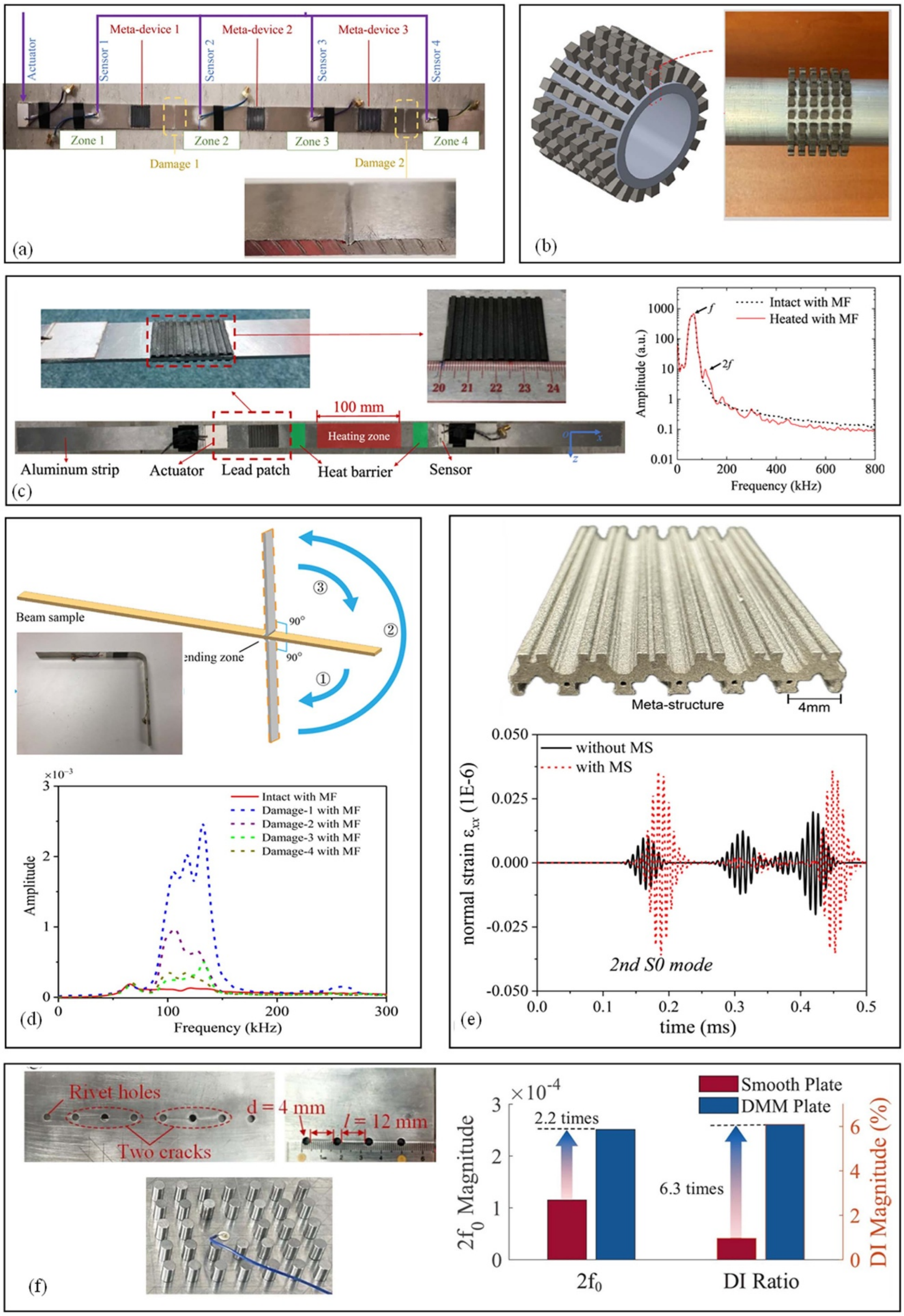

Figure 12. (a) Linear guided wave for crack detection [178], meta-filter-assisted detection for (b) corrosion [164], (c) thermal aging damage [160], and (d) plasticity evolution [157], (e) mode conversion-enabled (from A to S modes) material degradation detection [172], and (f) metamaterial-enhanced sensing for fatigue crack evaluation [181]. (a) Reprinted from [178], Copyright (2022), with permission from Elsevier. (b) Reproduced from [164]. CC BY 4.0. (c) Reproduced from [160]. © IOP Publishing Ltd All rights reserved. (d) Reproduced with permission from [157]. (e) Reprinted from [172], Copyright (2024), with permission from Elsevier. (f) Reprinted from [181], Copyright (2026), with permission from Elsevier.

5. Conclusions and future perspectives

This work presents a comprehensive review of state-of-the-art linear and nonlinear GW manipulation and GW-SHM techniques enhanced through integration with dedicatedly designed EMs. We start with a brief overview of linear and nonlinear GW theory, followed by a discussion of typical wave-manipulation functions that can be enabled by EMs, with emphasis on their underlying physical mechanisms. The review then examines the specific wave-manipulation requirements across all stages of a GW-SHM system, ranging from wave generation, propagation to sensing. Representative EM designs with salient physical features are presented and analyzed, highlighting their ability in improving damage detection sensitivity and robustness.

By engineering the bandgap properties of EMs, GWs can be selectively excited and transmitted with precise control over both frequency and wave mode. This capability enables the enhancement of interactions between target GW components and structural damage, thereby improving the sensitivity of GW-SHM systems. Furthermore, the strategic design of bandgap combinations using multiple EMs allows for the trapping of specific GW components in designated spatial regions, facilitating independent SHM operations across different structural zones. The wavefront shaping function enables the manipulation of GW propagation paths and the shaping of wavefronts. This functionality enhances GW energy density at specific locations, which is beneficial for both linear and nonlinear GW-SHM sensing applications. Additionally, the mode conversion ability inherent in EMs contributes to GW-SHM performance. By transferring energy from other wave modes, it enables the excitation of specialized wave modes that are traditionally challenging to generate, or amplifies the energy of desired GW modes to optimize SHM efficacy. Although advanced wave manipulation functionalities, such as topological modes and non-Hermitian PT symmetry, exhibit significant potential for damage detection, their practical integration into GW-SHM frameworks is still in the embryonic developing stage.

The integration of EMs not only offers a novel paradigm for advancing GW-SHM techniques but also drives innovations in EM research. The specific requirements for GW manipulation in GW-SHM inspire the development of new EM functionalities tailored to SHM needs. Moreover, since GW-SHM typically demands non-destructive EM configurations, it imposes harsher requirements and constraints on EM design, ultimately promoting the advancement of more sophisticated and practical EM design approaches. To propel the development of this emerging research frontier, greater efforts should be directed toward the following critical and interrelated aspects:

(1) ***Development of advanced EMs tailored for GW-SHM applications.*** A multitude of unresolved challenges persist in both linear and nonlinear GW-SHM, which underscores the need for more sophisticated and high-performance EM solutions. For instance, in finite-size engineering structures, Lamb wave fields become highly complex after long-distance propagation due to inherent issues such as wave beam divergence, boundary reflections, multi-mode coupling, and dispersion effects—these factors collectively degrade the clarity of damage-related signal features and make their identification and utilization more difficult. Nonlinear GW-SHM techniques, meanwhile, suffer from limited practical adoption due to their high susceptibility to environmental perturbations (e.g. temperature fluctuations, humidity), operational variability (e.g. varying loads), and instrumental noise, which undermine the reliability of nonlinear damage indicators. Furthermore, the conventional approach of simply bonding EMs to the host structure often faces practical limitations, such as poor durability and compatibility issues with complex structural geometries. To address these challenges, it is imperative to develop advanced EMs with enhanced wave manipulation performance to maximize the damage detection efficacy of GW-SHM systems. This would involve: (i) refining EM designs through state-of-the-art methodologies such as topological optimization, enabling precise tuning of wave interactions [185]; (ii) developing integrated configurations that embed EMs directly into host structures or transducers (e.g. co-fabrication with composite laminates), rather than relying on post-installed bonding [186, 187].

(2) ***Artificial intelligence (AI)-assisted inverse design of EMs for GWs.*** AI has emerged as a powerful tool for the inverse design of metamaterials, entailing remarkable improvements in design space and efficiency, optimization accuracy, and functional versatility. Such capability is particularly appealing for practical engineering applications, where rapid and targeted development of metamaterials is highly desirable, especially in SHM. Existing studies have already demonstrated the potential of AI-assisted inverse design in metamaterials [188–195]. In the field of EMs, AI-enabled inverse design has been employed to realize a variety of wave-control functionalities, including mode selection [196], anisotropic elastic property [197], dispersion relation customization [198], and other advanced

dynamic responses. Despite these advances, the application of AI-inverse-designed EMs to GW manipulation remains relatively limited. This gap restricts the broader integration of metamaterial-based wave control strategies into GW-SHM, where precise manipulation of wave modes, propagation paths, frequency content, energy density concentration, and damage-sensitive nonlinear features is essential. Therefore, the AI-driven inverse design of metamaterials specifically for guided-wave applications is a highly promising research direction. Future efforts should focus not only on achieving efficient wave control but also on integrating multiple design objectives simultaneously, such as broadband performance, compactness, and robustness to manufacturing uncertainties etc. Such developments are expected to give rise to next generation intelligent metamaterial-enabled GW-SHM systems with enhanced sensitivity, adaptability, and real-world applicability.

(3) ***Advancement of GW-SHM frameworks leveraging underutilized EM functionalities.*** A significant number of advanced wave manipulation capabilities inherent to EMs have yet to be harnessed in GW-SHM. For example, despite the promising potential of topological EM modes, known for their robust, defect-immune wave propagation, their application in damage detection and localization remains largely unexplored. Similarly, a range of unique wave phenomena enabled by EMs, including negative refraction [199, 200], wave cloaking [201–203], metasurface lens-based wave steering [138, 204], and non-reciprocal wave propagation [205, 206], have not been systematically integrated into GW-SHM workflows. These unconventional wave behaviors hold substantial promise for addressing longstanding GW-SHM limitations: they can enhance targeted wave-damage interactions (e.g. by focusing wave energy at critical structural hotspots) and mitigate interference from non-damage-related artifacts (e.g. suppressing boundary reflections or scattering from benign structural features). Moreover, by extracting and analyzing distinctive features from these EM-enabled wave phenomena, researchers can inversely drive the development of next-generation GW-SHM techniques—ones that offer superior damage sensitivity, robustness against environmental noise, and long-term reliability for real-world engineering applications.

(4) ***Consideration of specific requirements in realistic engineering contexts***. Deploying EM-based solutions for SHM applications is among the very first ventures in promoting metamaterial-based technology for engineering applications. Despite the promise shown, most of the studies have been carried out under well-controlled laboratory conditions, with most of the time, simplified and idealized structures and damage scenarios. Therefore, the proposed EM-based solution needs to be assessed in more realistic engineering contexts to identify existing weaknesses, formulate future development needs, and ultimately increase the technological readiness level of this promising technology. For example, the adaptation of the designed EMs to varying environments is a big challenge. This requires the tunability of EMs [207, 208], rather than passive structures. Furthermore, adaptive 'intelligent EMs', capable of performing real-time adjustment of their wave manipulation properties in response to varying operational or environmental condition changes [110, 111], can be developed.

Acknowledgment

The research was funded by grants from the National Natural Science Foundation of China (12302114), National Key Laboratory of Equipment State Sensing and Smart Support at National University of Defense Technology (WDZC20265290303), RIAIoT (Research Institute for Artificial Intelligence of Things) through project P0049625, the Research Grants Council of Hong Kong Special Administrative Region (PolyU 152013/21E), the Innovation and Technology Commission of the HKSAR Government to the Hong Kong Branch of National Rail Transit Electrification and Automation Engineering Technology Research Center (K-BBY1).

Data availability statement

All data that support the findings of this study are included within the article (and any supplementary files).

Author contributions

Shengbo Shan 0000-0002-0950-6193
Conceptualization (equal), Data curation (equal), Formal analysis (equal), Funding acquisition (equal), Investigation (equal), Resources (equal), Writing – original draft (equal)

Ze Liu 0000-0002-4565-4767
Conceptualization (equal), Data curation (equal), Formal analysis (equal), Investigation (equal), Writing – original draft (equal)

Yue-Sheng Wang 0000-0002-0043-8411
Investigation (equal), Supervision (equal), Writing – review & editing (supporting)

Li Cheng 0000-0001-6110-8099
Funding acquisition (equal), Investigation (equal), Resources (equal), Supervision (equal), Writing – review & editing (equal)

References

[1] Pruell C, Kim J-Y, Qu J and Jacobs L J 2009 Evaluation of fatigue damage using nonlinear guided waves *Smart Mater. Struct.* **18** 035003
[2] Deng M and Pei J 2007 Assessment of accumulated fatigue damage in solid plates using nonlinear Lamb wave approach *Appl. Phys. Lett.* **90** 121902
[3] Hong M, Su Z, Wang Q, Cheng L and Qing X 2014 Modeling nonlinearities of ultrasonic waves for fatigue damage characterization: theory, simulation, and experimental validation *Ultrasonics* **54** 770–8
[4] Pruell C, Kim J-Y, Qu J and Jacobs L J 2007 Evaluation of plasticity driven material damage using Lamb waves *Appl. Phys. Lett.* **91** 231911
[5] Xiang Y, Deng M, Liu C-J and Xuan F-Z 2015 Contribution of mixed dislocations to the acoustic nonlinearity in plastically deformed materials *J. Appl. Phys.* **117** 214903
[6] Sun X *et al* 2017 Simulations on monitoring and evaluation of plasticity-driven material damage based on second harmonic of S0 mode Lamb waves in metallic plates *Materials* **10** 827
[7] Cantrell J H 2009 Nonlinear dislocation dynamics at ultrasonic frequencies *J. Appl. Phys.* **105** 043520
[8] Cash W and Cai W 2011 Dislocation contribution to acoustic nonlinearity: the effect of orientation-dependent line energy *J. Appl. Phys.* **109** 014915
[9] Masserey B and Fromme P 2013 Fatigue crack growth monitoring using high-frequency guided waves *Struct. Health Monit.* **12** 484–93
[10] Falcó O, Lopes C, Sommer D, Thomson D, Ávila R and Tijs B 2022 Experimental analysis and simulation of low-velocity impact damage of composite laminates *Compos. Struct.* **287** 115278
[11] Giurgiutiu V 2014 *Structural Health Monitoring with Piezoelectric Wafer Active Sensors* (Academic)
[12] Farrar C R and Worden K 2007 An introduction to structural health monitoring *Phil. Trans. R. Soc. A* **365** 303–15
[13] Roy S, Lonkar K, Janapati V and Chang F-K 2014 A novel physics-based temperature compensation model for structural health monitoring using ultrasonic guided waves *Struct. Health Monit.* **13** 321–42
[14] Wang C H, Rose J T and Chang F-K 2004 A synthetic time-reversal imaging method for structural health monitoring *Smart Mater. Struct.* **13** 415
[15] Chang F-K, Markmiller J, Yang J and Kim Y (eds) 2001 *Structural Health Monitoring, System Health Management* (Wiley)
[16] Glisic B 2024 *Introduction to Strain-based Structural Health Monitoring of Civil Structures* (Wiley)
[17] Khoo L M, Mantena P R and Jadhav P 2004 Structural damage assessment using vibration modal analysis *Struct. Health Monit.* **3** 177–94
[18] Ono K 2018 Review on structural health evaluation with acoustic emission *Appl. Sci.* **8** 958
[19] Behnia A, Chai H K and Shiotani T 2014 Advanced structural health monitoring of concrete structures with the aid of acoustic emission *Constr. Build. Mater.* **65** 282–302
[20] Sodano H A 2007 Development of an automated eddy current structural health monitoring technique with an extended sensing region for corrosion detection *Struct. Health Monit.* **6** 111–9
[21] Annamdas V G M and Soh C K 2010 Application of electromechanical impedance technique for engineering structures: review and future issues *J. Intell. Mater. Syst. Struct.* **21** 41–59
[22] Giurgiutiu V and Bao J 2004 Embedded-ultrasonics structural radar for *in situ* structural health monitoring of thin-wall structures *Struct. Health Monit.* **3** 121–40
[23] Golub M V, Shpak A N, Mueller I, Fomenko S I and Fritzen C-P 2021 Lamb wave scattering analysis for interface damage detection between a surface-mounted block and elastic plate *Sensors* **21** 860
[24] Rose J L 2004 Ultrasonic guided waves in structural health monitoring *Key Eng. Mater.* **270** 14–21
[25] Yu L and Tian Z 2013 Lamb wave structural health monitoring using a hybrid PZT-laser vibrometer approach *Struct. Health Monit.* **12** 469–83
[26] Su Z, Ye L and Lu Y 2006 Guided Lamb waves for identification of damage in composite structures: a review *J. Sound Vib.* **295** 753–80
[27] Cawley P 2024 Guided waves in long range nondestructive testing and structural health monitoring: principles, history of applications and prospects *NDT&E Int.* **142** 103026
[28] Abuassal A, Kang L, Martinho L, Kubrusly A, Dixon S, Smart E, Ma H and Sanders D 2025 A review of recent advances in unidirectional ultrasonic guided wave techniques for nondestructive testing and evaluation *Sensors* **25** 1050
[29] Yu S, Luo K, Fan C, Fu K, Wu X, Chen Y and Zhang X 2025 Advancing spacecraft safety and longevity: a review of guided waves-based structural health monitoring *Reliab. Eng. Syst. Saf.* **254** 110586

[30] Lu Y, Ye L, Su Z, Zhou L and Cheng L 2009 Artificial neural network (ANN)-based crack identification in aluminum plates with Lamb wave signals *J. Intell. Mater. Syst. Struct.* **20** 39–49
[31] Wen F, Shan S and Cheng L 2021 Third harmonic shear horizontal waves for material degradation monitoring *Struct. Health Monit.* **20** 475–83
[32] Xu H, Liu L, Li X, Xiang Y and Xuan F-Z 2024 Wavefield imaging of nonlinear ultrasonic Lamb waves for visualizing fatigue micro-cracks *Ultrasonics* **138** 107214
[33] Shi L, Xu Q, Ren Y, Chen J, Qiu L and Yuan S 2025 A new guided wave array-summated gradient product index (SGPI) for monitoring invisible hole-edge crack in the aircraft attachment lug under time-varying conditions *Mech. Syst. Signal Process.* **238** 113153
[34] Li L and Fromme P 2024 Mode conversion of fundamental guided ultrasonic wave modes at part-thickness crack-like defects *Ultrasonics* **142** 107399
[35] Sun L, Wei J, Peng C, Hao W, Teng F, Fan L, Zhang L, Sui Q and Jiang M 2025 Ultrasonic guided wave-based probabilistic diagnostic imaging method with single-path-scattering sparse reconstruction for multi-damage detection in composite structures *Mech. Syst. Signal Process.* **223** 111858
[36] Zhao X, Gao H, Zhang G, Ayhan B, Yan F, Kwan C and Rose J L 2007 Active health monitoring of an aircraft wing with embedded piezoelectric sensor/actuatornetwork: i. Defect detection, localization and growth monitoring *Smart Mater. Struct.* **16** 1208
[37] Michaels J E 2008 Detection, localization and characterization of damage in plates with an *in situ* array ofspatially distributed ultrasonic sensors *Smart Mater. Struct.* **17** 035035
[38] Amjad U, Yadav S K and Kundu T 2015 Detection and quantification of pipe damage from change in time of flight and phase *Ultrasonics* **62** 223–36
[39] Tang H-Y, Winkelmann C, Lestari W and Saponara V L 2011 Composite structural health monitoring through use of embedded PZT sensors *J. Intell. Mater. Syst. Struct.* **22** 739–55
[40] Michaels T E, Michaels J E and Ruzzene M 2011 Frequency–wavenumber domain analysis of guided wavefields *Ultrasonics* **51** 452–66
[41] Tang R, Zhang S, Wu W, Zhang S and Han Z 2023 Explainable deep learning based ultrasonic guided wave pipe crack identification method *Measurement* **206** 112277
[42] Jing H, Yuan S, Chen J and Meng Y 2025 A multi-scale deep residual network-based guided wave imaging evaluation method for fatigue crack quantification *Meas. Sci. Technol.* **36** 016115
[43] Xiang Y, Deng M and Xuan F-Z 2014 Creep damage characterization using nonlinear ultrasonic guided wave method: a mesoscale model *J. Appl. Phys.* **115** 044914
[44] Shan S, Cheng L and Wen F 2018 Design of nonlinear-Lamb-wave-based structural health monitoring systems with mitigated adhesive nonlinearity *Smart Mater. Struct.* **27** 105006
[45] Wang R, Wu Q, Yu F, Okabe Y and Xiong K 2019 Nonlinear ultrasonic detection for evaluating fatigue crack in metal plate *Struct. Health Monit.* **18** 869–81
[46] Lissenden C J 2021 Nonlinear ultrasonic guided waves—principles for nondestructive evaluation *J. Appl. Phys.* **129** 021101
[47] Pan Y, Khodaei Z S and Aliabadi F 2025 Online fatigue crack detection and growth modelling through higher harmonic analysis: a baseline-free approach *Mech. Syst. Signal Process.* **224** 112167
[48] Liu Y, Wang M, Kundu T, Chen S, Li J, Zeng Z and Liu Y 2026 Effective stress monitoring in structures using sideband peak count-index of nonlinear guided waves *Ultrasonics* **161** 107951
[49] Deng M 1999 Cumulative second-harmonic generation of Lamb-mode propagation in a solid plate *J. Appl. Phys.* **85** 3051–8
[50] De Lima W and Hamilton M 2003 Finite-amplitude waves in isotropic elastic plates *J. Sound Vib.* **265** 819–39
[51] Alippi A, Bettucci A, Germano M and Passeri D 2006 Harmonic and subharmonic acoustic wave generation in finite structures *Ultrasonics* **44** e1313–e8
[52] Huang X, Qu W, Xiao L and Lu Y 2024 A subharmonic modulation-based approach for debonding damage detection of composite stiffened plates *Case Stud. Nondestruct. Test Eval.* **39** 802–31
[53] Sun X, Ding X, Li F, Zhou S, Liu Y, Hu N, Su Z, Zhao Y, Zhang J and Deng M 2018 Interaction of Lamb wave modes with weak material nonlinearity: generation of symmetric zero-frequency mode *Sensors* **18** 2451
[54] Nagy P B, Qu J and Jacobs L J 2013 Finite-size effects on the quasistatic displacement pulse in a solid specimen with quadratic nonlinearity *J. Acoust. Soc. Am.* **134** 1760–74
[55] Rollins F R Jr 1963 Interaction of ultrasonic waves in solid media *Appl. Phys. Lett.* **2** 147–8
[56] Hasanian M and Lissenden C J 2017 Second order harmonic guided wave mutual interactions in plate: vector analysis, numerical simulation, and experimental results *J. Appl. Phys.* **122** 084901
[57] Shan S and Cheng L 2020 Mode-mixing-induced second harmonic A0 mode Lamb wave for local incipient damage inspection *Smart Mater. Struct.* **29** 055020
[58] Ma P S, Lee H J and Kim Y Y 2015 Dispersion suppression of guided elastic waves by anisotropic metamaterial *J. Acoust. Soc. Am.* **138** EL77–EL82
[59] Liu Z, Shan S-B, Dong H-W and Cheng L 2022 Topologically customized and surface-mounted meta-devices for Lamb wave manipulation *Smart Mater. Struct.* **31** 065001
[60] Wen F, Shan S and Cheng L 2022 Immunity of the second harmonic shear horizontal waves to adhesive nonlinearity for breathing crack detection *Struct. Health Monit.* **21** 2340–53
[61] Kamal A and Giurgiutiu V 2014 Shear horizontal wave excitation and reception with shear horizontal piezoelectric wafer active sensor (SH-PWAS) *Smart Mater. Struct.* **23** 085019
[62] Miao H, Huan Q, Wang Q and Li F 2017 A new omnidirectional shear horizontal wave transducer using face-shear (d24) piezoelectric ring array *Ultrasonics* **74** 167–73
[63] Shan S, Cheng L and Li P 2016 Adhesive nonlinearity in Lamb-wave-based structural health monitoring systems *Smart Mater. Struct.* **26** 025019
[64] Sik Ma P, Eui Kwon Y and Young Kim Y 2013 Wave dispersion tailoring in an elastic waveguide by phononic crystals *Appl. Phys. Lett.* **103** 151901
[65] Shan S, Zhang Y, Cheng L, Song Y, Pan Y and Cheng L 2024 Cumulative effect' of second harmonic Lamb waves in a lossy plate *Ultrasonics* **138** 107229
[66] Salmanpour M, Khodaei Z S and Aliabadi M 2017 Transducer placement optimisation scheme for a delay and sum damage detection algorithm *Struct. Control Health Monit.* **24** e1898

[67] Song Y, Shan S, Zhang Y and Cheng L 2025 Physics-guided neural network for structural health monitoring with lamb waves through boundary reflection elimination *Struct. Health Monit.* **25** 1219–36
[68] Liu Z, Zhang X, Mao Y, Zhu Y Y, Yang Z, Chan C T and Sheng P 2000 Locally resonant sonic materials *Science* **289** 1734–6
[69] Feng L, Wong Z J, Ma R-M, Wang Y and Zhang X 2014 Single-mode laser by parity-time symmetry breaking *Science* **346** 972–5
[70] He C, Sun X-C, Liu X-P, Lu M-H, Chen Y, Feng L and Chen Y-F 2016 Photonic topological insulator with broken time-reversal symmetry *Proc. Natl Acad. Sci.* **113** 4924–8
[71] Yu N and Capasso F 2014 Flat optics with designer metasurfaces *Nat. Mater.* **13** 139–50
[72] Xie Y, Wang W, Chen H, Konneker A, Popa B-I and Cummer S A 2014 Wavefront modulation and subwavelength diffractive acoustics with an acoustic metasurface *Nat. Commun.* **5** 5553
[73] Fleury R, Sounas D L, Sieck C F, Haberman M R and Alù A 2014 Sound isolation and giant linear nonreciprocity in a compact acoustic circulator *Science* **343** 516–9
[74] Dong H-W, Zhao S-D, Wang Y-S, Cheng L and Zhang C 2020 Robust 2D/3D multi-polar acoustic metamaterials with broadband double negativity *J. Mech. Phys. Solids* **137** 103889
[75] Li S, Zhao D, Niu H, Zhu X and Zang J 2018 Observation of elastic topological states in soft materials *Nat. Commun.* **9** 1370
[76] Yu S-Y, He C, Wang Z, Liu F-K, Sun X-C, Li Z, Lu H-Z, Lu M-H, Liu X-P and Chen Y-F 2018 Elastic pseudospin transport for integratable topological phononic circuits *Nat. Commun.* **9** 3072
[77] Zhu R, Liu X, Hu G, Sun C T and Huang G 2014 Negative refraction of elastic waves at the deep-subwavelength scale in a single-phase metamaterial *Nat. Commun.* **5** 5510
[78] Chen Y, Hu G and Huang G 2017 A hybrid elastic metamaterial with negative mass density and tunable bending stiffness *J. Mech. Phys. Solids* **105** 179–98
[79] Liu Z, Qin K-Q and Yu G-L 2020 Partially embedded gradient metabarrier: broadband shielding from seismic Rayleigh waves at ultralow frequencies *J. Eng. Mech.* **146** 04020032
[80] Morini L, Eyzat Y and Gei M 2019 Negative refraction in quasicrystalline multilayered metamaterials *J. Mech. Phys. Solids* **124** 282–98
[81] Dong H-W, Zhao S-D, Wang Y-S and Zhang C 2017 Topology optimization of anisotropic broadband double-negative elastic metamaterials *J. Mech. Phys. Solids* **105** 54–80
[82] Liu Y, Su X and Sun C 2015 Broadband elastic metamaterial with single negativity by mimicking lattice systems *J. Mech. Phys. Solids* **74** 158–74
[83] Wang Y-F, Wang Y-S and Su X-X 2011 Large bandgaps of two-dimensional phononic crystals with cross-like holes *J. Appl. Phys.* **110** 113520
[84] Liu Z, Dong H-W, Yu G-L and Cheng L 2022 Achieving ultra-broadband and ultra-low-frequency surface wave bandgaps in seismic metamaterials through topology optimization *Compos. Struct.* **295** 115863
[85] Liu F, Zhang F, Wei W, Hu N, Deng G and Wang Z 2016 Scattering of waves by three-dimensional obstacles in elastic metamaterials with zero index *Phys. Rev. B* **94** 224102
[86] Chen Y, Li X, Nassar H, Norris A N, Daraio C and Huang G 2019 Nonreciprocal wave propagation in a continuum-based metamaterial with space-time modulated resonators *Phys. Rev. Appl.* **11** 064052
[87] Gong C, Fang X and Cheng L 2025 Band evolution and 2D nonreciprocal wave propagation in strongly nonlinear meta-plates *Nonlinear Dyn.* **113** 23999–4019
[88] Park J H, Ma P S and Kim Y Y 2015 Design of phononic crystals for self-collimation of elastic waves using topology optimization method *Struct. Multidiscip. Opt.* **51** 1199–209
[89] Chen Y, Li X, Nassar H, Hu G and Huang G 2018 A programmable metasurface for real time control of broadband elastic rays *Smart Mater. Struct.* **27** 115011
[90] Zhu H and Semperlotti F 2016 Anomalous refraction of acoustic guided waves in solids with geometrically tapered metasurfaces *Phys. Rev. Lett.* **117** 034302
[91] Chen A-L, Wang Y-S, Wang Y-F, Zhou H-T and Yuan S-M 2022 Design of acoustic/elastic phase gradient metasurfaces: principles, functional elements, tunability, and coding *Appl. Mech. Rev.* **74** 020801
[92] Zhou C, Hong M, Su Z, Wang Q and Cheng L 2012 Evaluation of fatigue cracks using nonlinearities of acousto-ultrasonic waves acquired by an active sensor network *Smart Mater. Struct.* **22** 015018
[93] Liu P, Sohn H, Kundu T and Yang S 2014 Noncontact detection of fatigue cracks by laser nonlinear wave modulation spectroscopy (LNWMS) *NDT&E Int.* **66** 106–16
[94] Achenbach J 2012 *Wave Propagation in Elastic Solids* (Elsevier)
[95] Rose J L 2014 *Ultrasonic Guided Waves in Solid Media* (Cambridge University Press)
[96] Giurgiutiu V 2005 Tuned Lamb wave excitation and detection with piezoelectric wafer active sensors for structural health monitoring *J. Intell. Mater. Syst. Struct.* **16** 291–305
[97] Liu Y, Chillara V K and Lissenden C J 2013 On selection of primary modes for generation of strong internally resonant second harmonics in plate *J. Sound Vib.* **332** 4517–28
[98] Murnaghan F D 1937 Finite deformations of an elastic solid *Am. J. Math.* **59** 235–60
[99] Landau L D, Pitaevskii L, Kosevich A M and Lifshitz E M 2012 *Theory of Elasticity* vol 7 (Elsevier)
[100] Brugger K 1964 Thermodynamic definition of higher order elastic coefficients *Phys. Rev.* **133** A1611
[101] Liu Z, Shan S and Cheng L 2024 A0 mode Lamb wave propagation in a nonlinear medium and enhancement by topologically designed metasurfaces for material degradation monitoring *Nonlinear Dyn.* **112** 16963–81
[102] Chillara V K and Lissenden C J 2014 Nonlinear guided waves in plates: a numerical perspective *Ultrasonics* **54** 1553–8
[103] Auld B A 1973 *Acoustic Fields and Waves in Solids* (Рипол Классик)
[104] Solodov I Y, Krohn N and Busse G 2002 CAN: an example of nonclassical acoustic nonlinearity in solids *Ultrasonics* **40** 621–5
[105] Broda D, Staszewski W J, Martowicz A, Uhl T and Silberschmidt V 2014 Modelling of nonlinear crack–wave interactions for damage detection based on ultrasound—a review *J. Sound Vib.* **333** 1097–118
[106] Allen J C P and Ng C T 2023 Damage detection in composite laminates using nonlinear guided wave mixing *Compos. Struct.* **311** 116805
[107] Wang K, Liu M, Su Z, Yuan S and Fan Z 2018 Analytical insight into "breathing" crack-induced acoustic nonlinearity with an application to quantitative evaluation of contact cracks *Ultrasonics* **88** 157–67
[108] Friswell M I and Penny J E 2002 Crack modeling for structural health monitoring *Struct. Health Monit.* **1** 139–48
[109] Gudmundson P 1983 The dynamic behaviour of slender structures with cross-sectional cracks *J. Mech. Phys. Solids* **31** 329–45

[110] Wu B, Jiang W, Jiang J, Zhao Z, Tang Y, Zhou W and Chen W 2024 Wave manipulation in intelligent metamaterials: recent progress and prospects *Adv. Funct. Mater.* **34** 2316745
[111] Qian C, Kaminer I and Chen H 2025 A guidance to intelligent metamaterials and metamaterials intelligence *Nat. Commun.* **16** 1154
[112] Guzman D G, Pillarisetti L S S, Sridhar S, Lissenden C J, Frecker M and Shokouhi P 2022 Design of resonant elastodynamic metasurfaces to control S Lamb waves using topology optimization *JASA Express Lett.* **2** 115601
[113] Giraldo Guzman D, Lissenden C, Shokouhi P and Frecker M 2023 Topology optimization design of resonant structures based on antiresonance eigenfrequency matching informed by harmonic analysis *J. Mech. Des.* **145** 101704
[114] Wang P, Chen T-N, Yu K-P and Wang X-P 2013 Lamb wave band gaps in a double-sided phononic plate *J. Appl. Phys.* **113** 053509
[115] Badreddine Assouar M and Oudich M 2012 Enlargement of a locally resonant sonic band gap by using double-sides stubbed phononic plates *Appl. Phys. Lett.* **100** 123506
[116] Yi J, Wu Z, Xia R and Li Z 2022 Reconfigurable metamaterial for asymmetric and symmetric elastic wave absorption based on exceptional point in resonant bandgap *Appl. Math. Mech.* **44** 1–20
[117] Hsu J-C and Wu T-T 2008 Calculations of Lamb wave band gaps and dispersions for piezoelectric phononic plates using mindlin's theory-based plane wave expansion method *IEEE Trans. Ultrason. Ferroelectr. Freq. Control* **55** 431–41
[118] Pillarisetti L, Guzman D G, Keirn J, Sridhar S, Lissenden C, Frecker M and Shokouhi P 2025 Frequency bandgap enhancement in locally resonant metasurfaces for S0 Lamb wave mode using topology-optimized resonators *J. Appl. Phys.* **137** 043104
[119] Hedayatrasa S, Kersemans M, Abhary K, Uddin M and Van Paepegem W 2018 Optimization and experimental validation of stiff porous phononic plates for widest complete bandgap of mixed fundamental guided wave modes *Mech. Syst. Signal Process.* **98** 786–801
[120] Hedayatrasa S, Abhary K, Uddin M and Ng C-T 2016 Optimum design of phononic crystal perforated plate structures for widest bandgap of fundamental guided wave modes and maximized in-plane stiffness *J. Mech. Phys. Solids* **89** 31–58
[121] Sun Y, Li C, Zheng H, Li X, Han Q and Yao X 2025 Topological tunability and wave manipulation of enhanced inertial-amplification-based metastructures *Phys. Rev. Appl.* **24** 024051
[122] Chen J, Xia Y, Han X and Zhang H 2012 Lamb waves in phononic crystal slabs: truncated plane parallels to the axis of periodicity *Ultrasonics* **52** 920–4
[123] Lott M, Roux P, Rupin M, Colquitt D and Colombi A 2021 Negative index metamaterial through multi-wave interactions: numerical proof of the concept of low-frequency Lamb-wave multiplexing *Sci. Rep.* **11** 561
[124] Kushwaha M S, Halevi P, Dobrzynski L and Djafari-Rouhani B 1993 Acoustic band structure of periodic elastic composites *Phys. Rev. Lett.* **71** 2022
[125] Economou E and Sigalas M 1994 Stop bands for elastic waves in periodic composite materials *J. Acoust. Soc. Am.* **95** 1734–40
[126] Akbari-farahani F and Ebrahimi-nejad S 2024 From defect mode to topological metamaterials: a state-of-the-art review of phononic crystals & acoustic metamaterials for energy harvesting *Sensors Actuators A* **365** 114871
[127] Kaina N, Causier A, Bourlier Y, Fink M, Berthelot T and Lerosey G 2017 Slow waves in locally resonant metamaterials line defect waveguides *Sci. Rep.* **7** 15105
[128] Wang Y-F, Yang L, Wang T-T, Chen A-L, Laude V and Wang Y-S 2021 Guided Lamb waves in reconfigurable phononic crystal waveguides *APL Mater.* **9** 081110
[129] Philippe F D, Murray T W and Prada C 2015 Focusing on plates: controlling guided waves using negative refraction *Sci. Rep.* **5** 11112
[130] Shao S, Chen J, Xia R and Li Z 2023 Lamb waves manipulation by piezoelectric metasurface with tunable diffraction orders *Front. Phys.* **10** 1114544
[131] Gérardin B, Laurent J, Legrand F, Prada C and Aubry A 2019 Negative reflection of elastic guided waves in chaotic and random scattering media *Sci. Rep.* **9** 2135
[132] Qiu H and Li F 2020 Manipulation of shear horizontal guided wave with arbitrary wave fronts by using metasurfaces *J. Phys. D: Appl. Phys.* **53** 285301
[133] Yu N, Genevet P, Kats M A, Aieta F, Tetienne J-P, Capasso F and Gaburro Z 2011 Light propagation with phase discontinuities: generalized laws of reflection and refraction *Science* **334** 333–7
[134] Liu Y, Liang Z, Liu F, Diba O, Lamb A and Li J 2016 Source illusion devices for flexural lamb waves using elastic metasurfaces (arXiv:1611.09650)
[135] Rong J, Ye W, Zhang S and Liu Y 2020 Frequency-coded passive multifunctional elastic metasurfaces *Adv. Funct. Mater.* **30** 2005285
[136] Cao L, Yang Z, Xu Y and Assouar B 2018 Deflecting flexural wave with high transmission by using pillared elastic metasurface *Smart Mater. Struct.* **27** 075051
[137] Lee J and Kim Y Y 2023 Elastic metamaterials for guided waves: from fundamentals to applications *Smart Mater. Struct.* **32** 123001
[138] Park C W and Kim Y Y 2025 Evolution of metasurfaces for advanced elastic wave manipulation: a comprehensive review *Smart Mater. Struct.* **34** 053003
[139] Yang X and Kim Y Y 2018 Topology optimization for the design of perfect mode-converting anisotropic elastic metamaterials *Compos. Struct.* **201** 161–77
[140] Lee J, Kweun M, Lee W, Park C I and Kim Y Y 2022 Perfect transmission of elastic waves obliquely incident at solid–solid interfaces *Extrem. Mech. Lett.* **51** 101606
[141] Chai Y, Yang X and Li Y 2023 Full mode-converting transmission between longitudinal and bending waves in plates and beams *J. Sound Vib.* **564** 117890
[142] Kweun J M, Lee H J, Oh J H, Seung H M and Kim Y Y 2017 Transmodal Fabry-Pérot resonance: theory and realization with elastic metamaterials *Phys. Rev. Lett.* **118** 205901
[143] De Ponti J M, Iorio L, Riva E, Ardito R, Braghin F and Corigliano A 2021 Selective mode conversion and rainbow trapping via graded elastic waveguides *Phys. Rev. Appl.* **16** 034028
[144] Ding T, Song A, Sun C, Xiang Y and Xuan F-Z 2022 Mode conversion of Lamb waves in a composite phononic crystal plate: numerical analysis and experimental validation *J. Appl. Phys.* **132** 225103
[145] Mousavi S H, Khanikaev A B and Wang Z 2015 Topologically protected elastic waves in phononic metamaterials *Nat. Commun.* **6** 8682

[146] Huang H, Chen J and Huo S 2017 Simultaneous topological Bragg and locally resonant edge modes of shear horizontal guided wave in one-dimensional structure *J. Phys. D: Appl. Phys.* **50** 275102
[147] Chen L and Nie G 2025 Topological edge state of lamb waves in pillared phononic crystal plates *Acta Mech. Solida Sin.* **39** 166–75 [In Chinese]
[148] An S, Liu T, Cao L, Gu Z, Fan H, Zeng Y, Cheng L, Zhu J and Assouar B 2024 Multibranch elastic bound states in the continuum *Phys. Rev. Lett.* **132** 187202
[149] Huang H, Chen J and Huo S 2021 Recent advances in topological elastic metamaterials *J. Phys.: Condens. Matter* **33** 503002
[150] Hatsugai Y 1993 Chern number and edge states in the integer quantum Hall effect *Phys. Rev. Lett.* **71** 3697
[151] Qian K, Apigo D J, Prodan C, Barlas Y and Prodan E 2018 Topology of the valley-Chern effect *Phys. Rev. B* **98** 155138
[152] Zak J 1989 Berry's phase for energy bands in solids *Phys. Rev. Lett.* **62** 2747
[153] Huang L, Huang S, Shen C, Yves S, Pilipchuk A S, Ni X, Kim S, Chiang Y K, Powell D A and Zhu J 2024 Acoustic resonances in non-Hermitian open systems *Nat. Rev. Phys.* **6** 11–27
[154] Mekrache K, Sainidou R, Rembert P, Stefanou N and Morvan B 2025 Observation of nonreciprocal propagation for guided Lamb modes in piezoelectric phononic crystals *J. Acoust. Soc. Am.* **158** 697–708
[155] Rosa M I N, Mazzotti M and Ruzzene M 2021 Exceptional points and enhanced sensitivity in PT-symmetric continuous elastic media *J. Mech. Phys. Solids* **149** 104325
[156] Yi J, Ma Z, Xia R, Negahban M, Chen C and Li Z 2022 Structural periodicity dependent scattering behavior in parity-time symmetric elastic metamaterials *Phys. Rev. B* **106** 014303
[157] Liu Z, Shan S and Cheng L 2023 Nonlinear-Lamb-wave-based plastic damage detection assisted by topologically designed metamaterial filters *Struct. Health Monit.* **22** 1828–43
[158] Ciampa F, Mankar A and Marini A 2017 Phononic crystal waveguide transducers for nonlinear elastic wave sensing *Sci. Rep.* **7** 14712
[159] Tian Y, Shen Y, Rao D and Xu W 2019 Metamaterial improved nonlinear ultrasonics for fatigue damage detection *Smart Mater. Struct.* **28** 075038
[160] Shan S, Wen F and Cheng L 2021 Purified nonlinear guided waves through a metamaterial filter for inspection of material microstructural changes *Smart Mater. Struct.* **30** 095017
[161] Sherwood G R, Chronopoulos D, Marini A and Ciampa F 2021 3D-printed phononic crystal waveguide transducers for nonlinear ultrasonic damage detection *NDT&E Int.* **121** 102456
[162] Aslam M and Lee J 2024 Numerical investigation of bandgap characteristics in integrated metallic metafilters for nonlinear guided wave applications *APL Mater.* **12** 111109
[163] Aslam M, Boris I and Lee J 2025 Eliminating PZT-induced harmonics using metasurface-based filters for enhanced nonlinear guided wave structural health monitoring *Mech. Syst. Signal Process.* **235** 112885
[164] Gao M, Ng C-T, Lin J and Kotousov A 2025 Damage detection in circular tubes using nonlinear ultrasonic guided waves with metasurface *Thin-Walled Struct.* **214** 113384
[165] Miniaci M, Gliozzi A S, Morvan B, Krushynska A, Bosia F, Scalerandi M and Pugno N M 2017 Proof of concept for an ultrasensitive technique to detect and localize sources of elastic nonlinearity using phononic crystals *Phys. Rev. Lett.* **118** 214301
[166] Song Y and Shen Y 2022 A metasurface radar for steering ultrasonic guided waves *J. Sound Vib.* **538** 117260
[167] Chen W, Hong X, Chen J, Yang D, Zhang A and Yue J 2025 S0 mode selective metamaterial-based ultrasonic guided wave damage detection in thin-walled metal plate *IEEE Trans. Instrum. Meas.* **74** 1–12
[168] Xia R, Wang W, Shao S, Wu Z, Chen J, Zhang X and Li Z 2023 Mode purification for multimode Lamb waves by shunted piezoelectric unimorph array *Appl. Phys. Lett.* **122** 201703
[169] Tian Y and Shen Y 2020 Selective guided wave mode transmission enabled by elastic metamaterials *J. Sound Vib.* **485** 115566
[170] Cao X, Jia C, Miao H, Kang G and Zhang C 2021 Excitation and manipulation of guided shear-horizontal plane wave using elastic metasurfaces *Smart Mater. Struct.* **30** 055013
[171] Sandeep Kumar S R, Krishnadas V K, Balasubramaniam K and Rajagopal P 2021 Waveguide metamaterial rod as mechanical acoustic filter for enhancing nonlinear ultrasonic detection *APL Mater.* **9** 061115
[172] Liu Z, Shan S and Cheng L 2024 Meta-structure enhanced second harmonic S0 waves for material microstructural changes monitoring *Ultrasonics* **139** 107295
[173] Liu Z, Shan S, Zhang C and Cheng L 2025 Effective generation of shear horizontal waves from Lamb waves by meta-converters *Mech. Syst. Signal Process.* **241** 113516
[174] Tian Y, Song Y, Shen Y and Yu Z 2022 A metamaterial ultrasound mode convertor for complete transformation of Lamb waves into shear horizontal waves *Ultrasonics* **119** 106627
[175] Shan S, Hasanian M, Cho H, Lissenden C J and Cheng L 2019 New nonlinear ultrasonic method for material characterization: codirectional shear horizontal guided wave mixing in plate *Ultrasonics* **96** 64–74
[176] Miao H, Huan Q and Li F 2016 Excitation and reception of pure shear horizontal waves by using face-shear d24 mode piezoelectric wafers *Smart Mater. Struct.* **25** 11LT01
[177] Hu H, Cui H, Yin X, Xu H and Yang T 2025 Boundary SH waves echo control of thin plate structures based on the gradient composite plate *Compos. Struct.* **373** 119617
[178] Shan S, Liu Z, Cheng L and Pan Y 2022 Metamaterial-enhanced coda wave interferometry with customized artificial frequency-space boundaries for the detection of weak structural damage *Mech. Syst. Signal Process.* **174** 109131
[179] Shan S, Liu Z, Zhang C, Cheng L and Pan Y 2024 A metamaterial-assisted coda wave interferometry method with nonlinear guided waves for local incipient damage monitoring in complex structures *Smart Mater. Struct.* **33** 035017
[180] Kudela P, Radzienski M, Miniaci M, Fiborek P and Ostachowicz W 2025 The design and testing of an ultrasensitive device with embedded phononic crystals for the detection and localisation of nonlinear guided waves *J. Sound Vib.* **611** 119155
[181] Tian Y, Fu H and Shen Y 2026 A defect-mode elastic metamaterial enhancing nonlinear ultrasonic signatures for fatigue crack detection *Mech. Syst. Signal Process.* **242** 113585
[182] Gliozzi A S, Miniaci M, Bosia F, Pugno N M and Scalerandi M 2015 Metamaterials-based sensor to detect and locate nonlinear elastic sources *Appl. Phys. Lett.* **107** 161902
[183] Tian Y, Fu H and Shen Y 2025 An elastic meta-enhancer for improved damage detection via nonlinear ultrasonic feature amplification *Mech. Syst. Signal Process.* **231** 112685
[184] Cao H, Li W, Wang Z, Tian F, Zhang L and Chen X 2023 Damage detection with single receiver by multidirectional dispersive phononic crystals *IEEE Trans. Instrum. Meas.* **72** 1–7
[185] Dong H-W *et al* 2024 Inverse design of phononic meta-structured materials *Mater. Today* **80** 824–55

[186] Hsu J-C and Wu T-T 2007 Lamb waves in binary locally resonant phononic plates with two-dimensional lattices *Appl. Phys. Lett.* **90** 201904

[187] Zhu R, Liu X, Huang G, Huang H H and Sun C 2012 Microstructural design and experimental validation of elastic metamaterial plates with anisotropic mass density *Phys. Rev. B* **86** 144307

[188] Yan J, Li Y, Yin G, Yao S and Peng Y 2025 Inverse design on customised absorption of acoustic metamaterials with high degrees of freedom by deep learning *Mech. Syst. Signal Process.* **237** 112989

[189] Zhang W and Zhao Y 2026 A new inverse design method for sound-absorbing metamaterial based on deep learning *Appl. Acoust.* **241** 111024

[190] Zheng X, Zhang X, Chen T-T and Watanabe I 2023 Deep learning in mechanical metamaterials: from prediction and generation to inverse design *Adv. Mater.* **35** 2302530

[191] Mohammadnejad M, Montazeri A, Bahmanpour E and Mahnama M 2024 Artificial neural networks for inverse design of a semi-auxetic metamaterial *Thin-Walled Struct.* **200** 111927

[192] Zhou W, Wang S, Wu Q, Xu X, Huang X, Huang G, Liu Y and Fan Z 2023 An inverse design paradigm of multi-functional elastic metasurface via data-driven machine learning *Mater. Des.* **226** 111560

[193] Xiao L, Cao Z, Lu H, Cai Y and Zhang Z 2023 *Optimal Design of One-dimensional Elastic Metamaterials through Deep convolutional Neural Network and Genetic Algorithm, Structures* (Elsevier) p 105349

[194] Liu C-X and Yu G-L 2023 Deep learning for the design of phononic crystals and elastic metamaterials *J. Comput. Des. Eng.* **10** 602–14

[195] Jin Y, He L, Wen Z, Mortazavi B, Guo H, Torrent D, Djafari-rouhani B, Rabczuk T, Zhuang X and Li Y 2022 Intelligent on-demand design of phononic metamaterials *Nanophotonics* **11** 439–60

[196] Zhang J, Cheng J, Li E and Li B 2025 Data-driven inverse design framework for broadband mode-selective elastic metasurfaces *Int. J. Mech. Sci.* **309** 111008

[197] Fu Z, Mao H and Yin B 2025 Inverse design of lattice metamaterials for fully anisotropic elastic constants: a data-driven and gradient-based method *Compos. Struct.* **359** 118975

[198] Jiang W, Zhu Y, Yin G, Lu H, Xie L and Yin M 2022 Dispersion relation prediction and structure inverse design of elastic metamaterials via deep learning *Mater. Today Phys.* **22** 100616

[199] Eleftheriades G V and Balmain K G 2005 *Negative-refraction Metamaterials: Fundamental Principles and applications* (Wiley)

[200] Wu Y, Lai Y and Zhang Z-Q 2011 Elastic metamaterials with simultaneously negative effective shear modulus and mass density *Phys. Rev. Lett.* **107** 105506

[201] Farhat M, Guenneau S and Enoch S 2009 Ultrabroadband elastic cloaking in thin plates *Phys. Rev. Lett.* **103** 024301

[202] Ning L, Wang Y-Z and Wang Y-S 2020 Active control cloak of the elastic wave metamaterial *Int. J. Solids Struct.* **202** 126–35

[203] Zhang H, Chen Y, Liu X and Hu G 2020 An asymmetric elastic metamaterial model for elastic wave cloaking *J. Mech. Phys. Solids* **135** 103796

[204] Cao L, Yang Z and Xu Y 2018 Steering elastic SH waves in an anomalous way by metasurface *J. Sound Vib.* **418** 1–14

[205] Nassar H, Yousefzadeh B, Fleury R, Ruzzene M, Alù A, Daraio C, Norris A N, Huang G and Haberman M R 2020 Nonreciprocity in acoustic and elastic materials *Nat. Rev. Mater.* **5** 667–85

[206] Trainiti G and Ruzzene M 2016 Non-reciprocal elastic wave propagation in spatiotemporal periodic structures *New J. Phys.* **18** 083047

[207] Wang Y-F, Wang Y-Z, Wu B, Chen W and Wang Y-S 2020 Tunable and active phononic crystals and metamaterials *Appl. Mech. Rev.* **72** 040801

[208] Wang Z, Zhang Q, Zhang K and Hu G 2016 Tunable digital metamaterial for broadband vibration isolation at low frequency *Adv. Mater.* **28** 9857–61